SIMULATION OF THE EXTINCTION EFFICIENCY, THE ABSORPTION EFFICIENCY AND THE ASYMMETRY FACTOR OF ICE CRYSTALS AND RELEVANT APPLICATIONS TO THE STUDY OF CIRRUS CLOUD RADIATIVE PROPERTIES

A Thesis

by

KAI LU

Submitted to the Office of Graduate Studies of
Texas A&M University
in partial fulfillment of the requirements for the degree of

MASTER OF SCIENCE

August 2010

Major Subject: Atmospheric Sciences

SIMULATION OF THE EXTINCTION EFFICIENCY, THE ABSORPTION EFFICIENCY AND THE ASYMMETRY FACTOR OF ICE CRYSTALS AND RELEVANT APPLICATIONS TO THE STUDY OF CIRRUS CLOUD RADIATIVE PROPERTIES

A Thesis

by

KAI LU

Submitted to the Office of Graduate Studies of
Texas A&M University
in partial fulfillment of the requirements for the degree of

MASTER OF SCIENCE

Approved by:

Chair of Committee,	Ping Yang
Committee Members,	George Kattawar
	Shaima Nasiri
Head of Department,	Kenneth Bowman

August 2010

Major Subject: Atmospheric Sciences

ABSTRACT

Simulation of the Extinction Efficiency, the Absorption Efficiency and the Asymmetry Factor of Ice Crystals and Relevant Applications to the Study of Cirrus Cloud Radiative Properties. (August 2010)

Kai Lu, B.S., Nanjing University of Information Science and Technology

Chair of Advisory Committee: Dr. Ping Yang

The single-scattering properties of six non-spherical ice crystals, droxtals, plates, solid columns, hollow columns, aggregates and 6-branch bullet rosettes are simulated. The anomalous diffraction theory (ADT) is applied to the simulation of the extinction efficiency and the absorption efficiency. Because the first order reflection is considered, the accuracy of the absorption efficiency increases with the increasing of the size parameter. Compared with the reference single-scattering properties from an improved geometric optics method (IGOM), the errors in the extinction and absorption efficiencies are small. In addition, the asymmetry factor is formulated within the framework of diffraction and external reflection. The asymmetry factor based on the ADT matches very well with the IGOM counterpart when the absorption is strong, but needs an improvement in the solar region.

The errors in conjunction with the application of the ADT-based optical properties to the computation of atmospheric fluxes and heating rates, based on the Fu-Liou model also are investigated. Two cases, one for tropical cirrus clouds and the other for mid-latitude cirrus clouds, are designed. It is found that the errors of bulk asymmetry

factor between ADT-based and IGOM-based result in an overestimation of downward infrared (IR) fluxes and upward solar fluxes, and an underestimation of upward IR fluxes and downward solar fluxes. The errors of the fluxes and heating rates based on two sets of single-scattering properties are caused mainly by the underestimation of the bulk absorption efficiency based on ADT. It is also shown that ADT-based optical properties generate more accurate radiative properties for tropical cirrus clouds than for the mid-latitude cirrus clouds. In conclusion, the ADT-based method can generate reasonably accurate single-scattering properties of ice crystals, and can result in reasonable upward IR and solar fluxes at top of atmosphere (TOA), downward IR fluxes at the surface, and net heating rates.

ACKNOWLEDGMENTS

I thank my advisor, Dr. Ping Yang, for supporting and guiding my research at Texas A&M University. I also thank Mr. Lei Bi and Dr. Gang Hong for their enormous help.

TABLE OF CONTENTS

Page

LIST OF FIGURES

Page

Page

Page

Page

LIST OF TABLES

Page

1. INTRODUCTION

Cirrus clouds cover large areas of the globe and are one of the important components in weather and climate research (Liou, 1986). They have been observed to cover approximate 20% of the global surface regularly and are composed of ice crystals. In addition, ice crystals scatter solar radiation, and absorb, scatter and emit infrared (hereafter IR) radiation (Liou, 1986), cirrus clouds usually give rise to a greenhouse effect (i.e. the positive forcing) in the IR region, but a cooling effect (i.e. the negative forcing) in the solar region at the surface (Zhang et al., 1999).

The climate effects of cirrus clouds and their changes are not so clear because there are still many uncertainties on the microphysical properties of cirrus clouds. The observations on the microphysics of cirrus clouds have only been conducted for a few decades because cirrus clouds reside in the upper troposphere. Observational studies via advanced technological instruments, radars and lidars, placed on planes and orbiting satellites (Weichmann, 1945, 1947; Heymsfield and Knollenberg, 1972; Heymsfield, 1975a, 1975b, and 1975c; Hobbs et al., 1975; Varley et al., 1978-1980) show that the shapes of ice crystals in cirrus clouds are exclusively non-spherical (Weichmann, 1945) and have been categorized into the following shapes: droxtals, bullets, rosettes, columns, and plates. To understand the importance of cirrus clouds microphysical effects on their radiative properties, Mishchenko et al. (1996a and 1996b) examined the sensitivity of the optical properties of hexagonal and spherical ice crystals and found that large errors would be generated in retrieving cloud optical thickness using spherical models instead of

---

This thesis follows the style of *Journal of the Atmospheric Sciences*.

non-spherical ones. Therefore, to get more accurate radiative properties of cirrus clouds, the optical properties of non-spherical ice particles are necessary.

Since cirrus clouds play an important role in the global radiative budget, the optical properties of non-spherical ice particles have thus been a focus of discussion. Many rigorous methods (e.g., Yang et al., 2000; 2005) have been developed to calculate the accurate optical properties; however, those methods are very time-consuming. The ADT method is computationally efficient for computing the extinction and absorption efficiencies. Therefore, ADT is applied in this study.

The ADT method, first introduced by van de Hulst in 1957, is based on two assumptions. The first assumption is that the refractive index of light scattering is close to 1, which guarantees that the propagating direction and the polarization configurations of the internal field within the particles do not significantly change. The second assumption is that the size parameter $x = \pi d / \lambda$ (d is the diameter, and λ is the wavelength) should be much larger than 1, which guarantees the traceability of geometric optical rays in a scattering particle. The ADT method has been successfully applied to the calculation of the extinction and absorption efficiencies in the shape of spheres (van de Hulst, 1957; Mitchell, 2000; Fu and Sun, 2001; Yang et al., 2005). Mitchell (2000) improved the ADT method by adding three missing physical processes: internal reflection, photon tunneling and edge diffraction. The ADT method has also been applied to other regular non-spherical shapes: hexagons, spheroids, and circular cylinders (Liu et al., 1998; Yang and Liou, 1997; Chýlek and James, 1991a and 1991b).

The ADT method has been proven to be a reasonably accurate and efficient approximation method to calculate the extinction and absorption efficiencies. After generating the asymmetry factors, the radiative properties can be computed. The

motivation of the study is to apply the ADT method to simulate the extinction efficiency, absorption efficiency and asymmetry factors of six non-spherical ice crystals and check the impacts of ADT assumption to the radiative transfer calculation involving cirrus clouds.

In this study, we develop an efficient modeling capability based on the ADT method for the calculation of the single-scattering properties of six non-spherical ice crystals, including droxtals, 6-branch bullet rosettes, solid hexagon columns, hollow hexagons columns, aggregates and plates. Since the refractive indices of ice are not close to 1 at most wavelengths, the first order reflection is considered. The inclusion of the first order reflection enhances the accuracy of the absorption efficiency in the case of large size parameters. The present effort not only provides the extinction and absorption efficiencies, but also computes the asymmetry factor. The asymmetry factor is calculated from the phase functions that contains the contributions from the first-order reflection and diffraction. To assess the errors of the ADT result in radiative transfer simulation involving ice clouds, the Fu-Liou model (Fu, 1991) is employed to compute atmospheric fluxes and heating rates. The single-scattering properties of six non-spherical ice particles calculated by more rigorous methods (IGOM, Yang et al., 2001; 2004) are used as reference (hereafter, referred to as the database). In the following Section 2, the methodology is discussed. The single-scattering properties of ice crystals for the six non-spherical shapes are presented in Section 3. Section 4 reports on atmospheric fluxes and heating rates based on the Fu-Liou model. The summary of this study is given in Section 5.

2. METHODOLOGY

The ADT method, which possesses a time-efficient advantage over other rigorous methods, is applied to calculate the single-scattering properties of six non-spherical ice crystal shapes: droxtals, 6-branch bullet rosettes, solid hexagon columns, hollow hexagons columns, aggregates and plates. Fu-Liou model (Fu, 1991) is an efficient radiative model that can be used to calculate atmospheric fluxes and heating/cooling rates. In this section, some background information is provided concerning the anomalous diffraction theory for the computation of the single-scattering properties of ice crystals and the Fu-liou model for the calculation of the radiative fluxes and the heating/cooling rates.

2.1 ADT

The ADT is a time-efficient method to calculate the extinction and absorption efficiencies. It is assumed that the real part of refractive index is close to 1 ($m > 1$) and the size parameter is much larger than 1 ($x = 2\pi a/\lambda >> 1$, where a is the particle radius and λ is the wavelength). Mitchell (2000) profoundly discussed on the disadvantages of ADT and pointed out that in the calculation of the Lorenz-Mie extinction and absorption coefficients, ADT omitted the following important physical processes: internal reflection/refraction, photon tunneling and edge diffraction. In our study, the ADT is applied to the six non-spherical shapes (shown in Fig. 1). The size distributions are also from the observations. Our study considers the first-order reflection in the ADT and thus

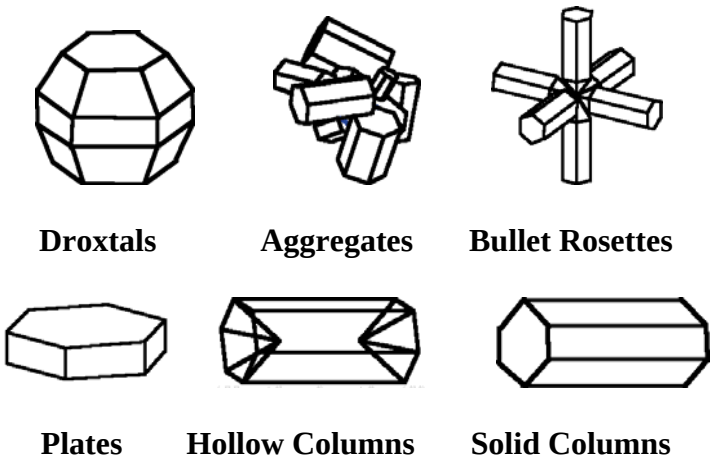

Figure 1 Six non-spherical ice crystal shapes (after Yang et al., 2005)

the absorption efficiency should be better fitted when the size parameter is much larger than 1. In addition, the asymmetry factor is formulated.

According to the original ADT theory, the extinction cross section is expressed as (van de Hulst, 1957)

$$\sigma_{ext} = 2\,\mathrm{Re}\left\{\iint_P [1 - e^{ikl(m-1)}]dP\right\} = 2\iint_p \left\{1 - e^{-iklm_i}\cos[kl(m_r - 1)]\right\}dP\,, \qquad (1)$$

and the absorption cross section is expressed as (van de Hulst, 1957)

$$\sigma_{abs} = \iint_P (1 - e^{-2klm_i})dP\,, \qquad (2)$$

where m_r and m_i indicate the real and imaginary parts of the complex refractive index m, respectively; $k = 2\pi/\lambda$, λ is the incident wavelength. As shown in Fig. 2, P is the projected cross section of the particle, and l is the propagation distance within the particle. One assumption of the ADT method is that the refractive index should be near 1; however at most wavelengths, the refractive indices of ice do not satisfy the condition. Therefore, the first-order reflection is taken into account in the computation of the ADT method.

Equation (2) is modified as

$$\sigma_{abs} = \iint_P (1 - e^{-2klm_i})dP \bullet (1 - R)\,. \qquad (3)$$

where R is the reflectance and is calculated by the formula in Yang and Liou (1995)

$$R = \frac{(R_a \bullet E_a)^2 + (R_b \bullet E_b)^2}{E_a{}^2 + E_b{}^2}\,. \qquad (4)$$

m_r is the real part of refractive indices.

To obtain the asymmetry factor, the phase function must be derived. We consider the phase function in the framework of diffraction and reflection. In that case, the phase function can be approximated as

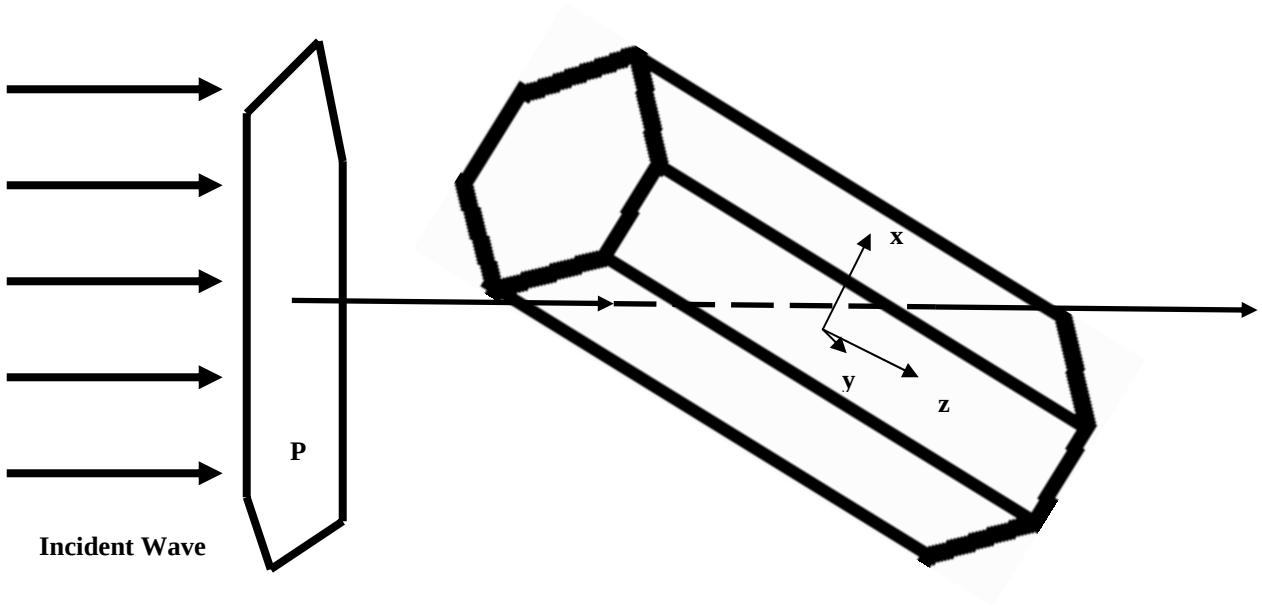

Figure 2 Geometric configurations illustrating the principle of the anomalous diffraction theory

$$P(\theta) = w_{dif}\ P_{dif}(\theta) + w_{refl} P_{refl}(\theta)\,. \tag{5}$$

where P_{dif} represents the normalized phase function associated with diffraction, and P_{refl} represents the normalized phase function associated with the first-order reflection. In this study, the projected area of non-spherical particles in the diffraction phase function is assumed to be spherical and the non-spherical particles are randomly oriented.

Considering from the energy region, the cross section for the diffraction is approximated as $0.5\sigma_e$ and the cross section for the reflection is $(0.5\sigma_e\text{-}\sigma_a)$. The sum of the scattering cross section is $(\sigma_e - \sigma_a)$. Therefore, the weighting of reflection w_{refl} can be expressed as

$$w_{refl} = \frac{0.5\sigma_e - \sigma_a}{\sigma_e - \sigma_a}\,. \tag{6}$$

w_{dif} is the weighting of diffraction and is given by

$$w_{dif} = \frac{0.5\sigma_e}{\sigma_e - \sigma_a}, \tag{7}$$

The phase function associated with diffraction and reflection can be expressed as

$$P_{dif}(\theta) \propto \left[\frac{2J_1(ka\sin\theta)}{ka\sin\theta}\right]^2 (1+\cos^2\theta)(1+\cos\theta)^2, \tag{8}$$

$$P_{refl}(\theta) \propto \left(\left|R_{\|}\right|^2 + \left|R_{\perp}\right|^2\right), \qquad . \tag{9}$$

$$R_{\|} = \frac{m_r\cos\theta_i - \cos\theta_t}{m_r\cos\theta_i + \cos\theta_t}, \qquad R_{\perp} = \frac{\cos\theta_i - m_r\cos\theta_t}{\cos\theta_i + m_r\cos\theta_t}, \tag{10}$$

where θ is the scattering angle, k is equal to $2\pi/\lambda$, $a = \sqrt{A/\pi}$, A is the projected area and J_1 is the first order Bessel function of the first kind. $R_{\|}$ and $R_{\perp}$ are the Fresnel reflection coefficients for the two polarization configurations (Yang et al., 2001). For randomly

oriented large particles and spheres with the same surface area and refractive index, the reflection patterns are the same, so $R_{\parallel}$ and $R_{\perp}$ can be computed with the analytical solutions in the case of normal incidence.

The asymmetry factor can be calculated via the following equation:

$$g = \frac{\int \cos\theta \bullet P(\theta) d(\cos\theta)}{\int P(\theta) d(\cos\theta)} . \quad . \tag{11}$$

2.2 Fu-Liou model

The Fu-Liou model (Fu, 1991) is a radiative transfer model used to calculate the atmospheric fluxes and heating rates in the plane parallel and vertically non-homogeneous atmosphere. It divides the entire spectrum (from 0.2 μm to 2,000,000 μm) into 18 bands: 6 bands in the solar region and 12 bands in the IR region (see Table 1). The model can calculate the radiative properties in the presence of clouds. Fu-Liou model is also suitable to the simulation of the atmospheric fluxes and heating/cooling rates with one or several layers of aerosols. These aerosols include marine aerosols, continental aerosols, urban aerosols, dusts, soot, sea salts, and sulfate droplets. In the present study, the errors of radiative fluxes and heating/cooling rates using the simulated and reference optical properties are examined.

Table 1 The spectral division of the Fu-Liou model bands (Fu, 1991)

	Band No.	Spectral Division
the Solar Region	1	0.2 μm – 0.7 μm
	2	0.7 μm – 1.3 μm
	3	1.3 μm – 1.9 μm
	4	1.9 μm – 2.5 μm
	5	2.5 μm – 3.5 μm
	6	3.5 μm – 4.0 μm
the IR Region	7	2200 cm^{-1} – 1900 cm^{-1}
	8	1900 cm^{-1}-1700 cm^{-1}
	9	1700 cm^{-1}-1400 cm^{-1}
	10	1400 cm^{-1}-1250 cm^{-1}
	11	1250 cm^{-1}-1100 cm^{-1}
	12	1100 cm^{-1}-980 cm^{-1}
	13	980 cm^{-1}-800 cm^{-1}
	14	800 cm^{-1}-670 cm^{-1}
	15	670 cm^{-1}-540 cm^{-1}
	16	540 cm^{-1}-400 cm^{-1}
	17	400 cm^{-1}-280cm^{-1}
	18	280 cm^{-1}-0 cm^{-1}

3. SCATTERING PROPERTIES OF ICE CRYSTALS BASED ON ANOMALOUS DIFFRACTION THEORY

To compute the single-scattering properties of ice crystals, the real parts and imaginary parts of refractive index are required. Figure 3 shows the real part of the complex refraction index of ice crystals (Warren and Brandt, 2008). It is evident that the real part of refractive index varies greatly in the wavelength ranging from 0.1 μm to 100 μm. When the wavelength is smaller than 100 μm, the real parts of refractive index are relatively small, and when the wavelength is larger than 1000 μm, the real parts of ice refractive index are relatively large and can be treated as a constant of 1.8. Figure 4 illustrates the imaginary part of refraction of ice from 0.1 μm to 2 μm. The larger the imaginary part of refractive index is, the stronger absorber the bulk material is. Therefore, it is evident that ice is a good absorber of the ultraviolet radiation, which wavelength is shorter than 0.16 μm. Ice is transparent to most of the solar radiation (from 0.2 μm to 2.5 μm) although there are some absorption regions in the solar region. In the IR region, imaginary part of ice refractive index varies about 0.1, which can be used to partly explain the warming effects of cirrus clouds. From Figures 3 and 4, it is shown that the refractive index of ice is not close to 1, so that the traditional ADT is not so appropriate to calculate the extinction and absorption efficiencies. Therefore, it is necessary to consider the first-order reflection.

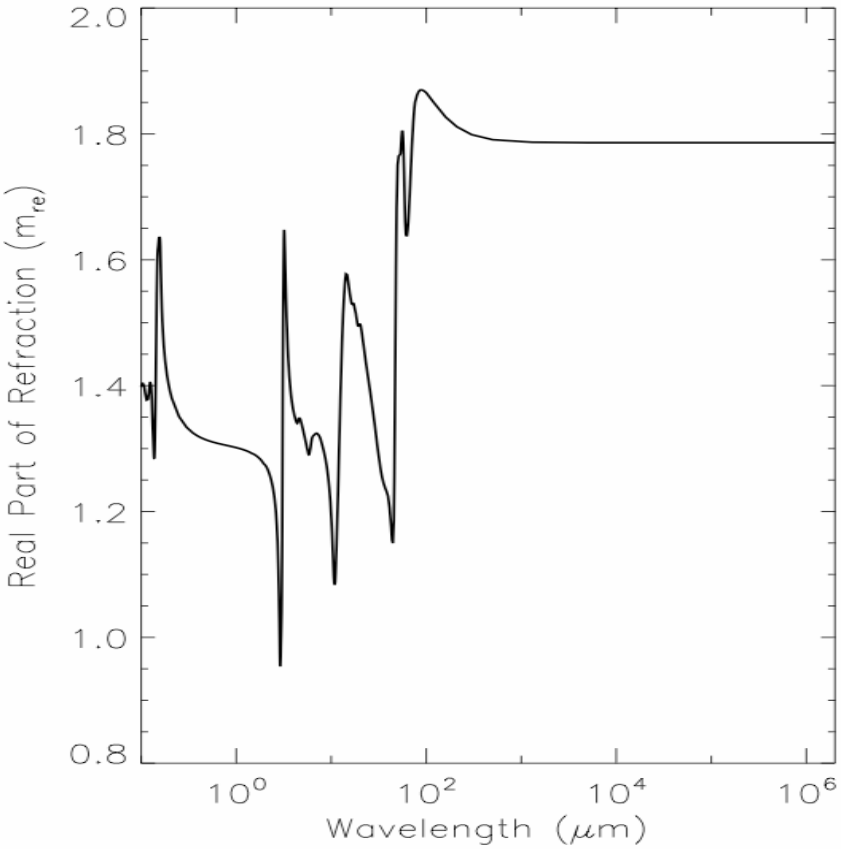

Figure 3 Real part of the complex index of refraction of ice (Warren and Brandt, 2008)

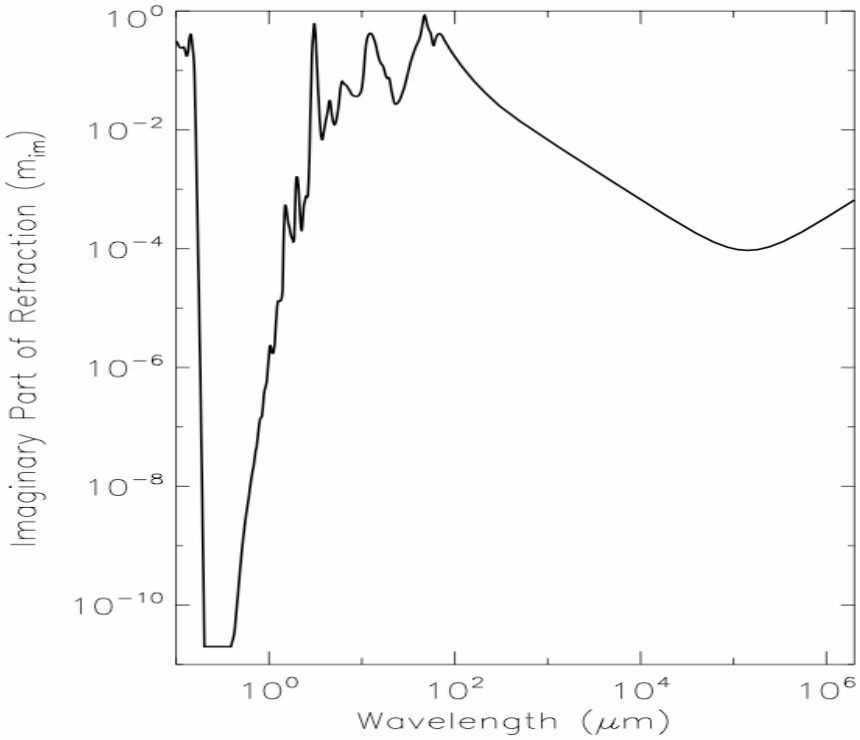

Figure 4 Imaginary part of the complex index of refraction of ice (Warren and Brandt, 2008**)**

3.1 Extinction efficiency

Figures 5 to 10 show the extinction efficiencies of solid columns, plates, bullets, aggregates, hollow columns and droxtals. The ADT-based the extinction efficiency is reasonably accurate compared with IGOM data. The shorter the wavelength is, the better the simulated results based on ADT match with the reference results based on IGOM. In the solar region, (e.g. 0.5 μm and 1.2 μm) the results calculated by the ray-by-ray method under the modified ADT assumptions match perfectly with those by the rigorous method (IGOM). The relative errors of two sets of extinction efficiencies are always under 3.4%. As for the extinction efficiencies at 3.5 μm, the ADT-based method can give rather accurate results compared with IGOM. In the IR region, using the modified ADT conditions, the ray-by-ray method can still generate the extinction efficiencies quite close to the IGOM-based extinction efficiencies. The underestimation of ADT-based result is always under 6% when size parameter is larger than 40. Noticeably, in the IR region and when the size parameter is small, there are some differences. That is because in the modified ADT the ray passes the scattering particles without the changes of propagation direction. In the reality, a ray should change its direction and even undergo several internal reflections in a non-spherical particle. The errors in the propagation distances generate the errors shown in these figures and have some relations with the refractive index and the particle shape. Comparing the cases of solid hexagons at 11 μm and 12 μm, m_r changes from 1.1 to 1.2 (Table 2), the maximum errors extend from 0.2 to 0.4. It is evident that there is a positive relation between the value of m_r and the errors. m_i also is positively related to the underestimation errors when judging the underestimation errors

Table 2 Refractive indices of ice crystals

Wavelength(μm)	m_r	m_i
0.5	1.313	5.88E-10
1.2	1.29	6.7E-6
3.5	1.45	1.5E-2
10	1.19	5.0E-2
11	1.08	2.48E-1
12	1.3	4.0E-1

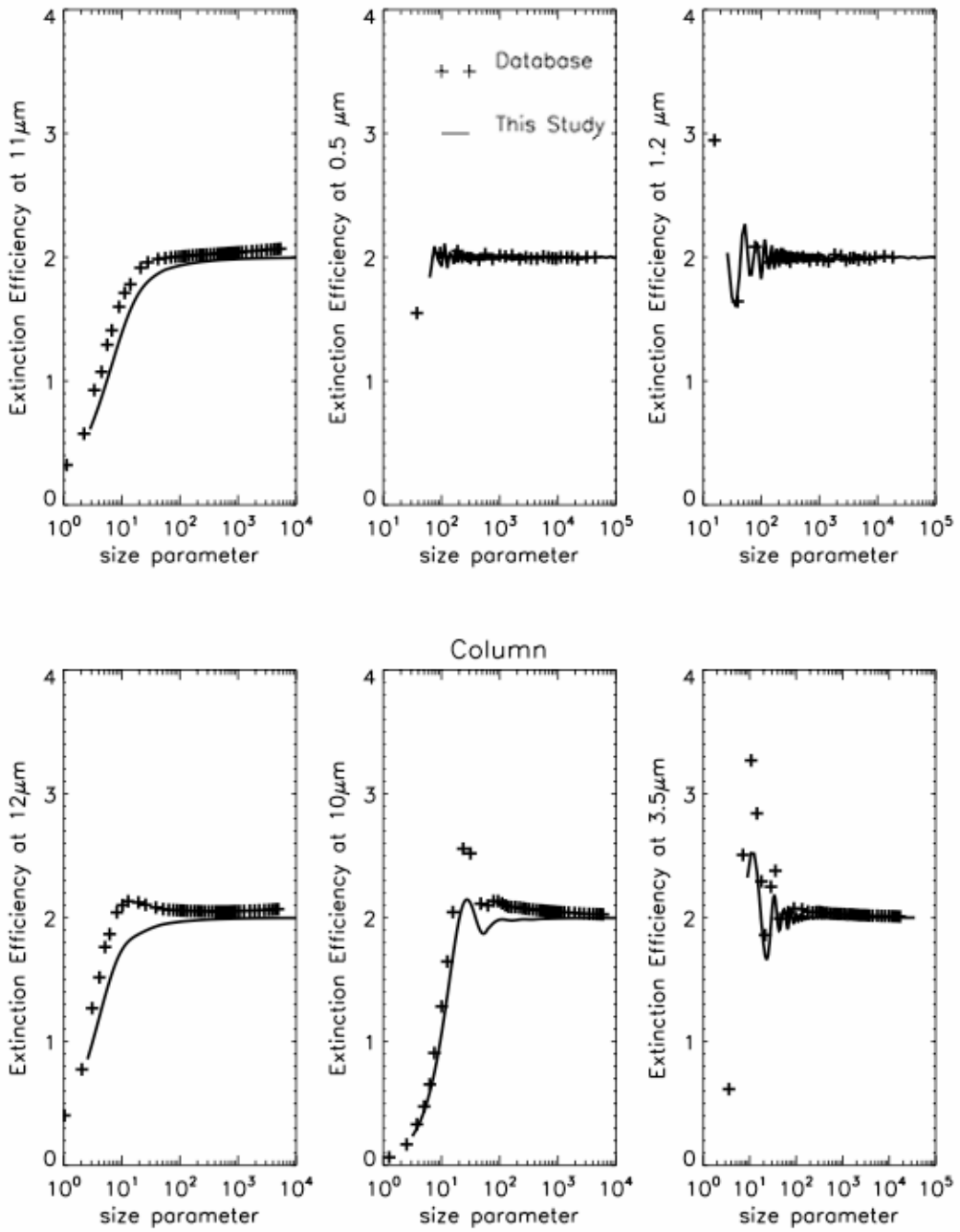

Figure 5 Extinction efficiencies of solid columns calculated using ray-by-ray method with the assumptions of ADT-based (solid lines) and from the database (plus signs). The definitions of the solid column shape can be found in Yang et al., 2000

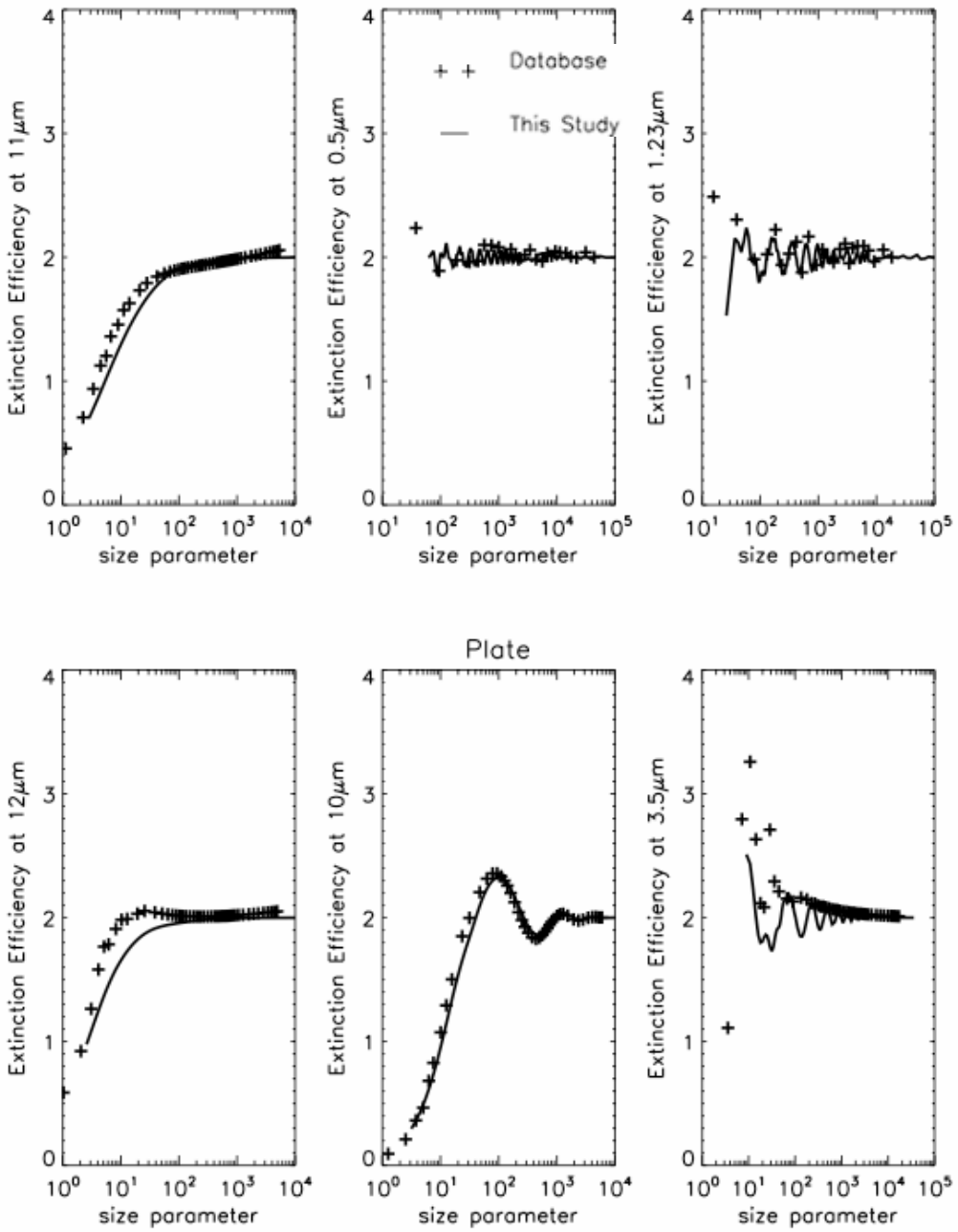

Figure 6 Extinction efficiencies of plates calculated using ray-by-ray method with the assumptions of ADT-based (solid lines) and from the database (plus signs). The definitions of the solid column shape can be found in Yang et al., 2000

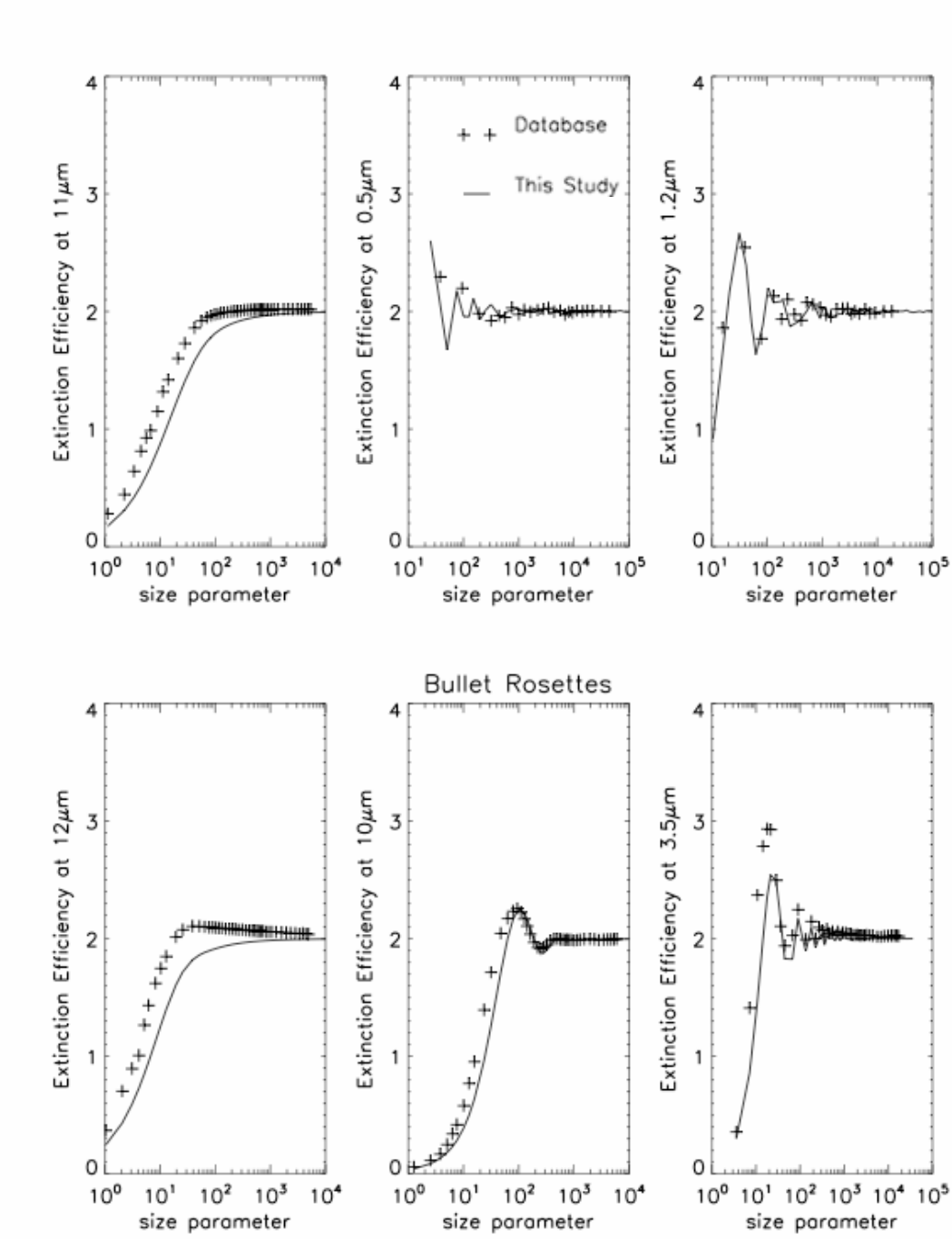

Figure 7 Extinction efficiencies of bullet rosettes calculated using ray-by-ray method with the assumptions of ADT-based (solid lines) and from the database (plus signs). The definitions of the solid column shape can be found in Yang et al., 2000

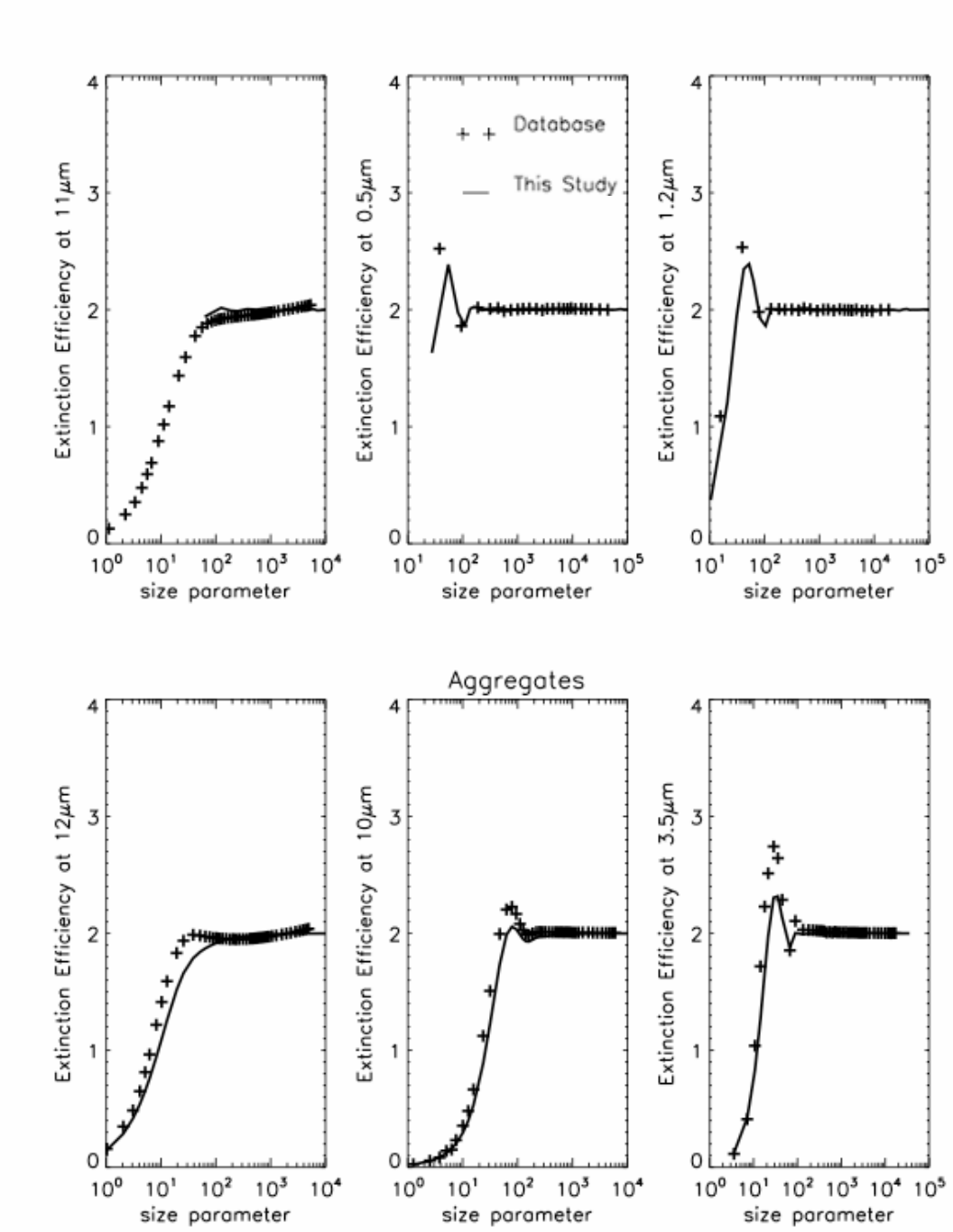

Figure 8 Extinction efficiencies of aggregates calculated using ray-by-ray method with the assumptions of ADT-based (solid lines) and from the database (plus signs). The definitions of the solid column shape can be found in Yang et al., 2000

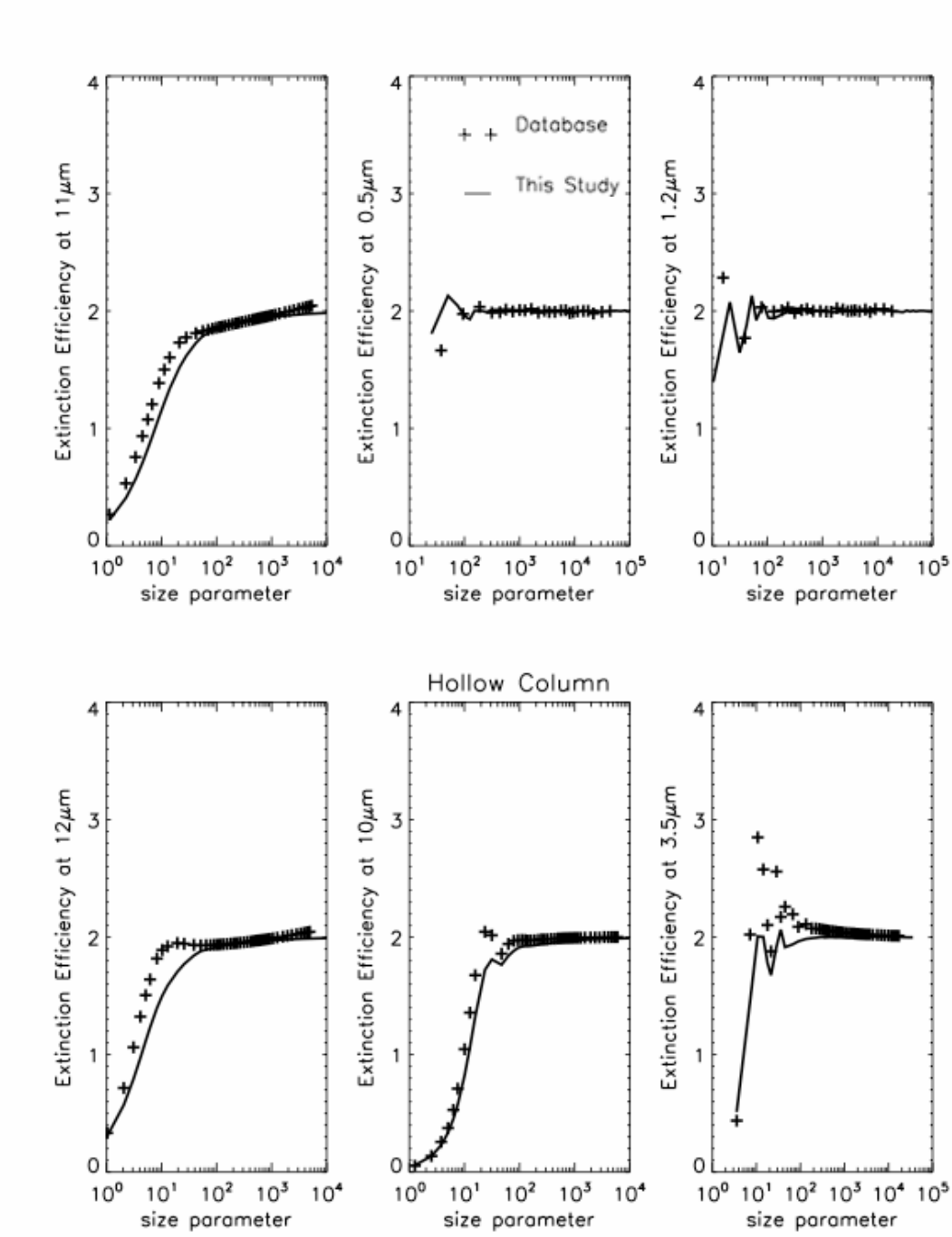

Figure 9 Extinction efficiencies of hollow columns calculated using ray-by-ray method with the assumptions of ADT-based (solid lines) and from the database (plus signs). The definitions of the solid column shape can be found in Yang et al., 2000

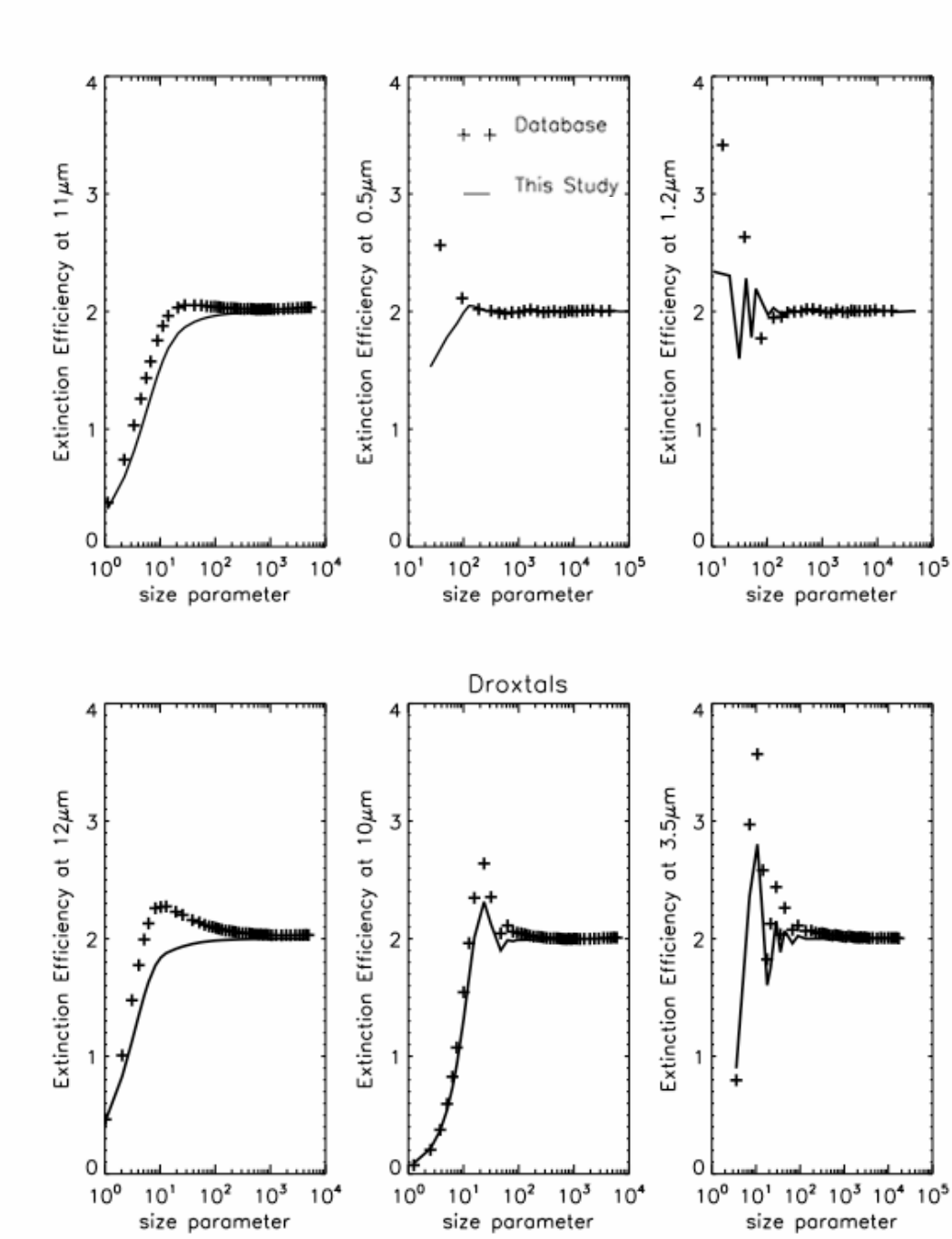

Figure 10 Extinction efficiencies of droxtals calculated using ray-by-ray method with the assumptions of ADT-based (solid lines) and from the database (plus signs). The definitions of the solid column shape can be found in Yang et al., 2005

of the extinction efficiency of plates at 10 μm and 12 μm. We should also notice that the shapes of non-spherical particles are an important factor to the errors in extinction efficiency. It can be shown that the errors of extinction efficiency of plates are much smaller than those of solid hexagons. It can be explained in this way: due to the flat-shape of plates, propagation distance in the particle decreases, and thus errors between ADT-based and IGOM-based caused by internal reflection become smaller significantly. Therefore, the underestimation of the ray is much smaller. In short, the ADT-based method can be used to generate the extinction efficiency of non-spherical ice particles.

3.2 Absorption efficiency

Figures 11 to 16 illustrate the absorption efficiencies of the six non-spherical ice particles. The most impressive differences against the original ADT method are that the absorption efficiency approaches to the transmittance when the size parameters are increasing. No matter the shapes of ice particles are solid columns, plates, bullets, aggregates, hollow columns or droxtals, the simulated absorption efficiency based on ADT is in a close agreement with the IGOM-based data when size parameter is large. In the shortwave region, the imaginary part of refractive index is close to 0, which means that ice particles scatter the sunlight with negligible absorption. Therefore, at 0.5 μm and 1.23 μm, the values of the absorption efficiencies are basically close to 0. As for the cases in the near infrared (3.5 μm) results calculated based on the ADT for six non-spherical shapes are underestimated as compared with the reference IGOM data and so do they at other wavelengths (10 μm,11 μm and 12 μm)in the IR regions. The relative errors

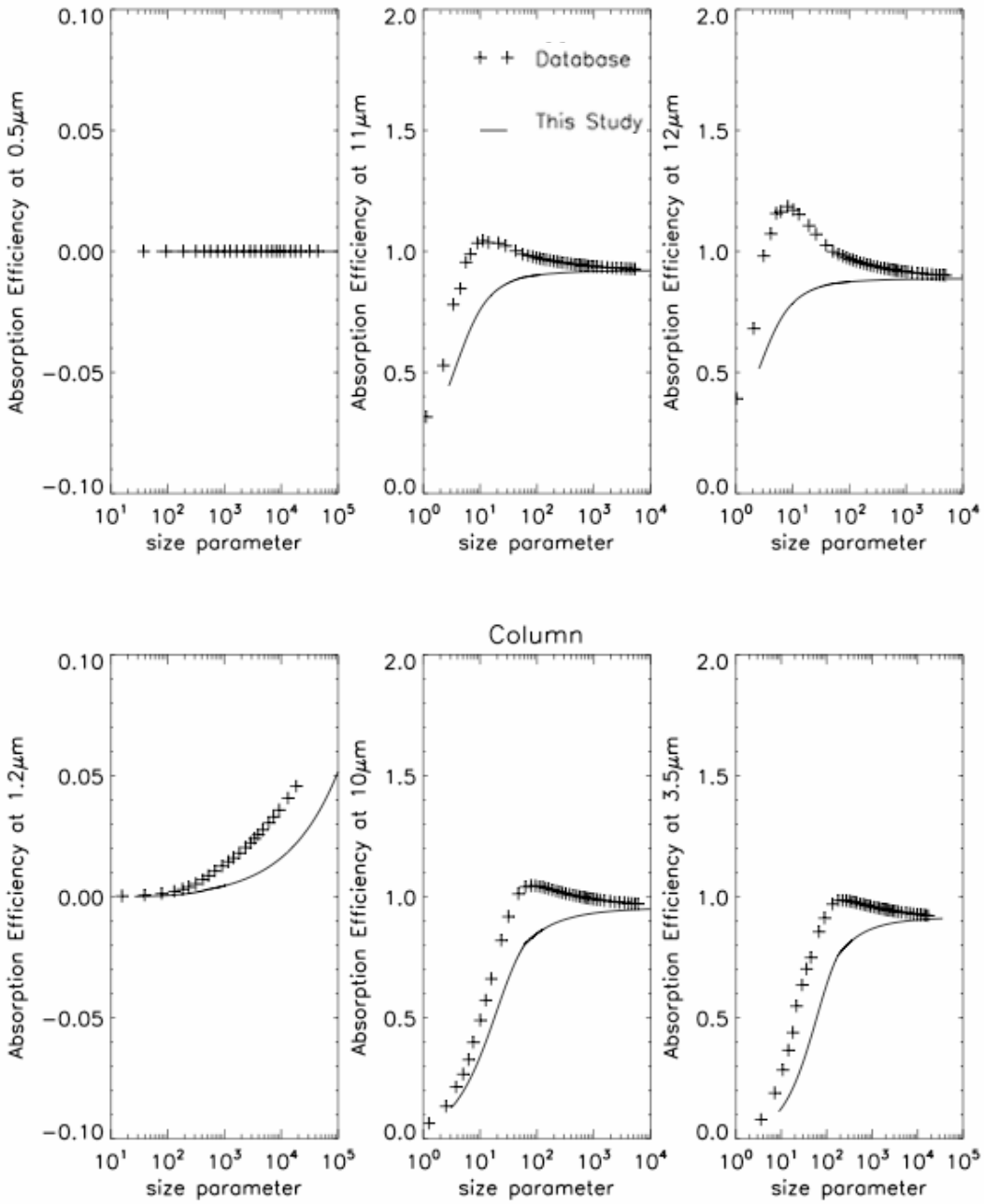

Figure 11 Absorption efficiencies of solid columns calculated using ray-by-ray method with the assumptions of ADT-based (solid lines) and from the database (plus signs). The definitions of the solid column shape can be found in Yang et al., 2000

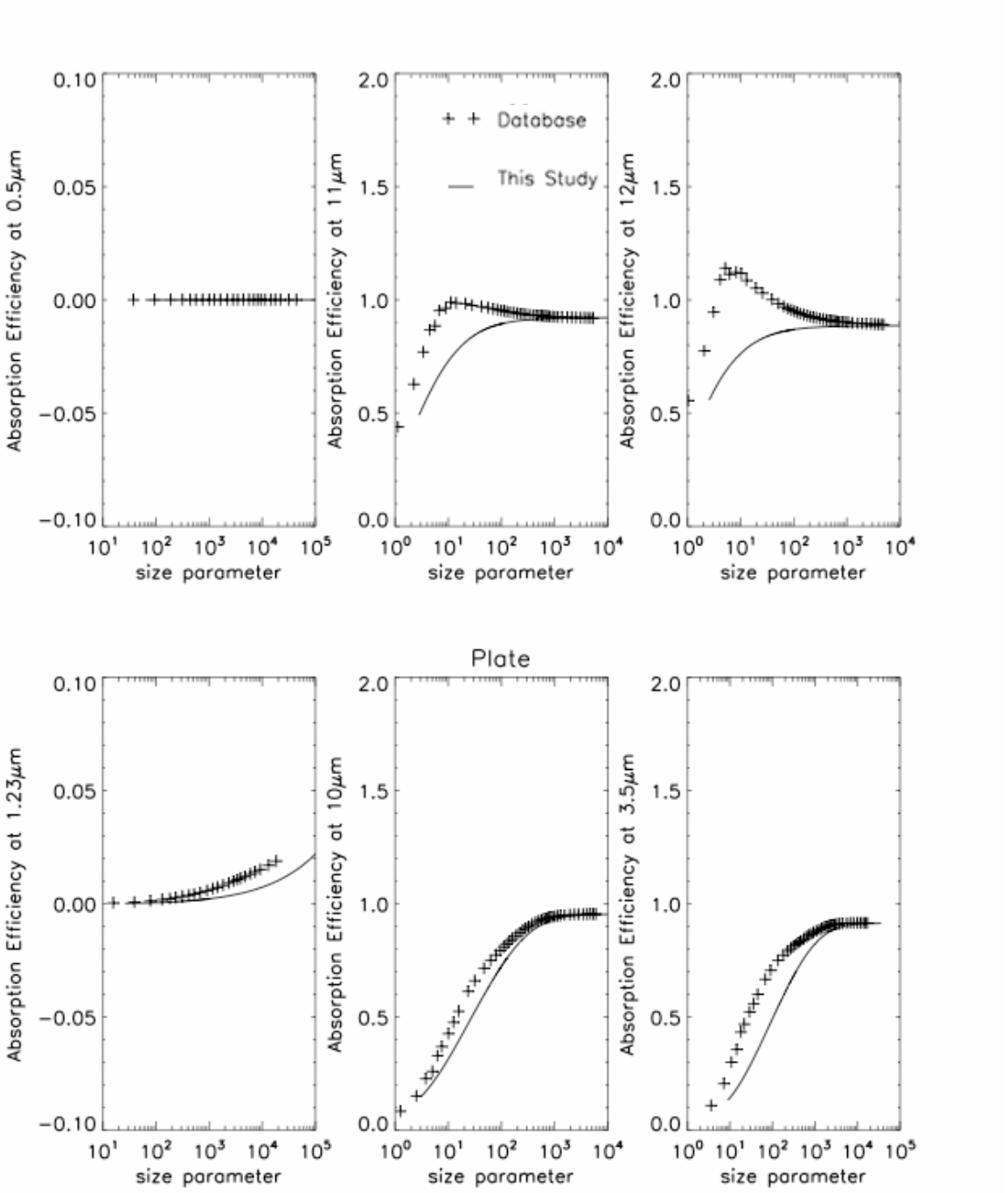

Figure 12 Absorption efficiencies of plates calculated using ray-by-ray method with the assumptions of ADT-based (dashed lines) and from the database (solid lines). The definitions of the solid column shape can be found in Yang et al., 2000

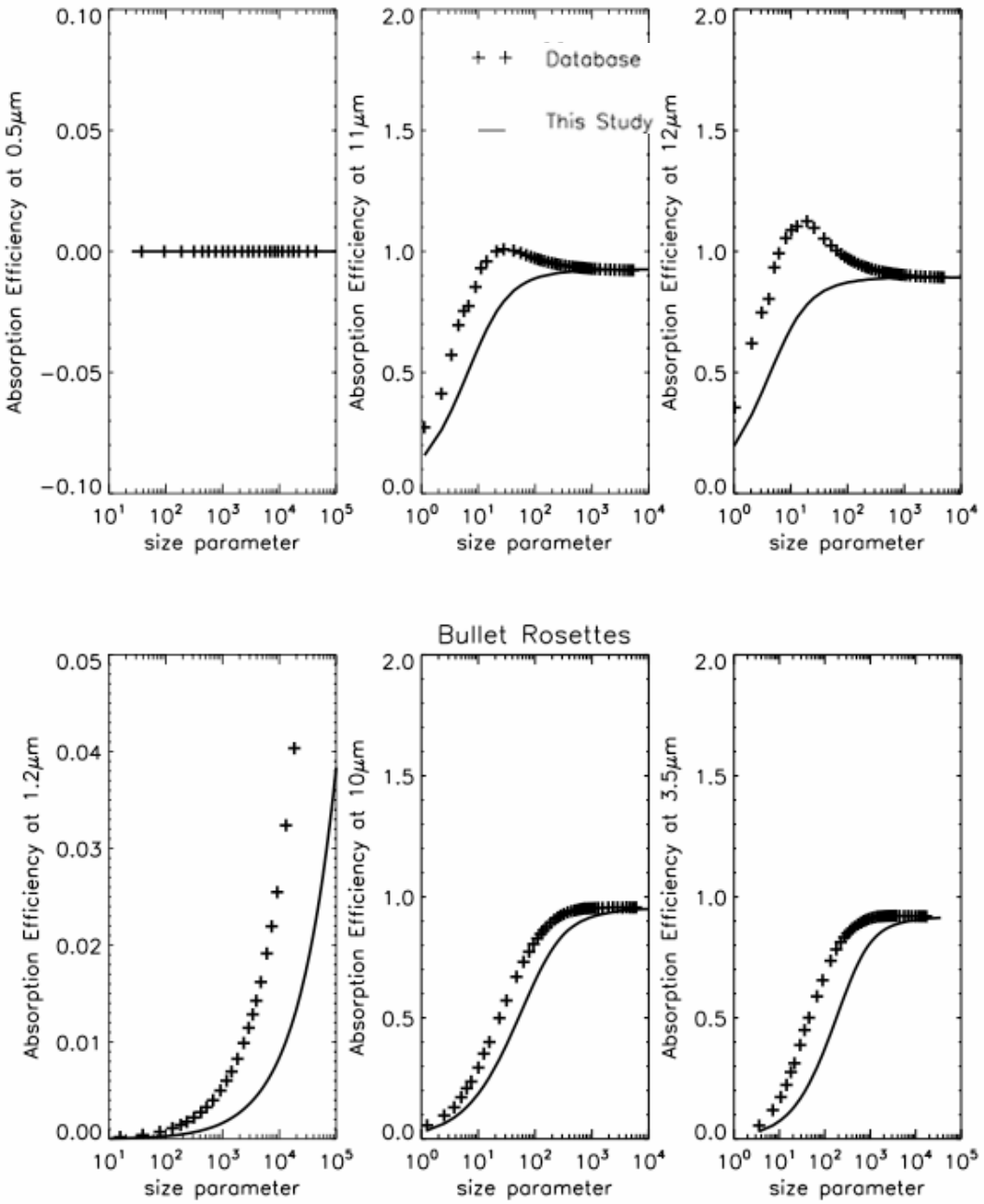

Figure 13 Absorption efficiencies of bullet rosettes calculated using ray-by-ray method with the assumptions of ADT-based (dashed lines) and from the database (solid lines). The definitions of the solid column shape can be found in Yang et al., 2000

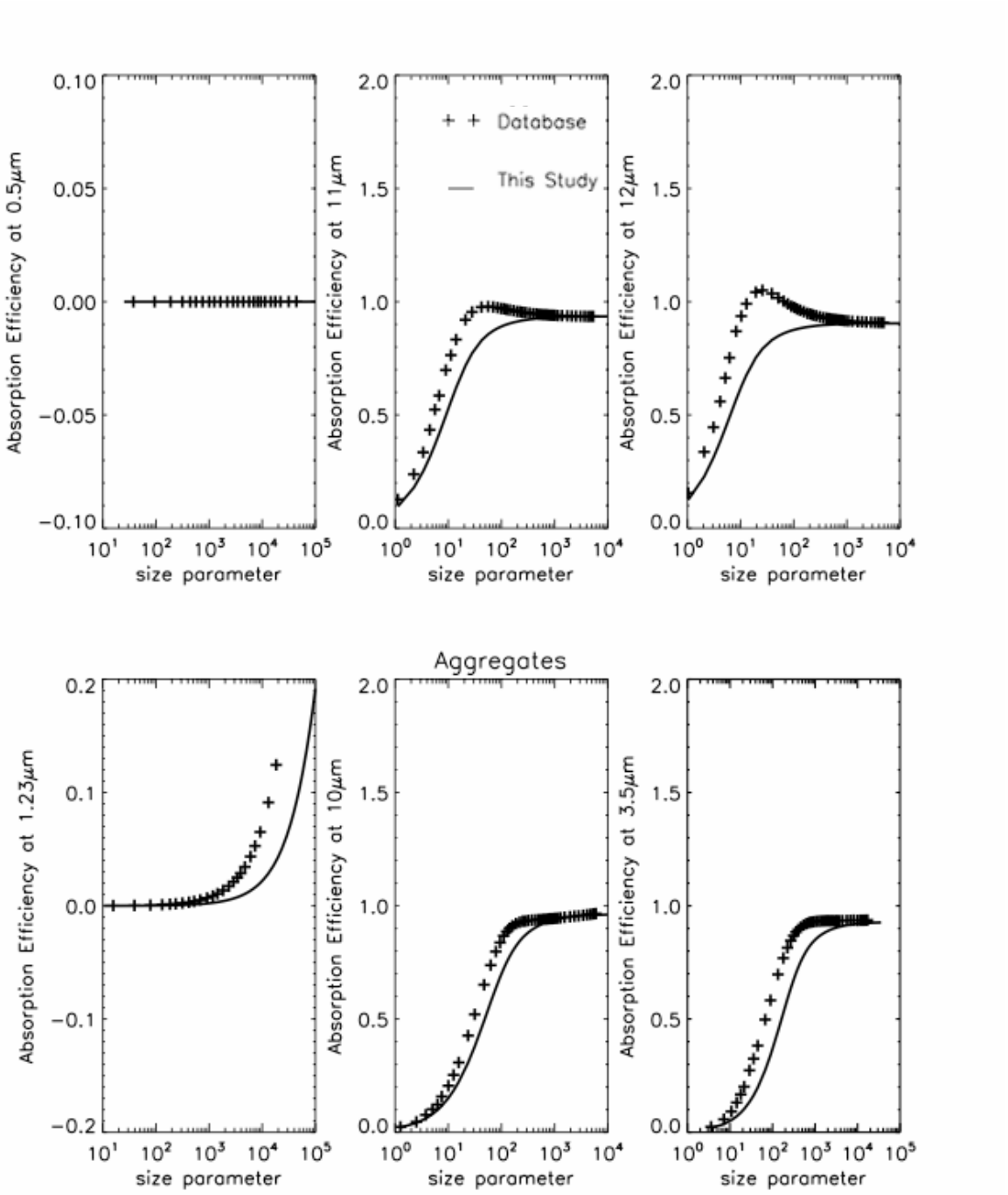

Figure 14 Absorption efficiencies of aggregates calculated using ray-by-ray method with the assumptions of ADT-based (dashed lines) and from the database (solid lines). The definitions of the solid column shape can be found in Yang et al., 2000

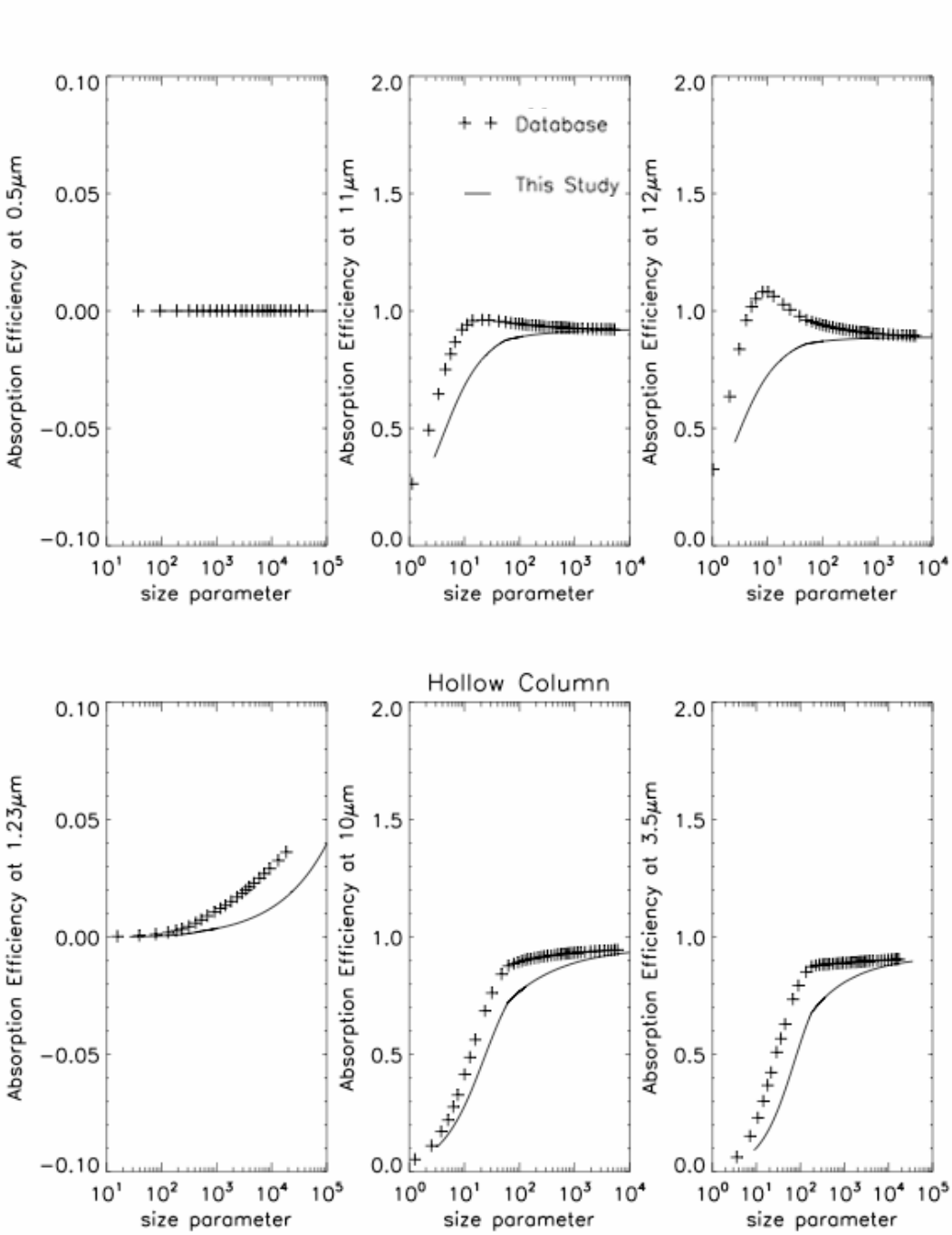

Figure 15 Absorption efficiencies of hollow columns calculated using ray-by-ray method with the assumptions of ADT-based (dashed lines) and from the database (solid lines). The definitions of the solid column shape can be found in Yang et al., 2000

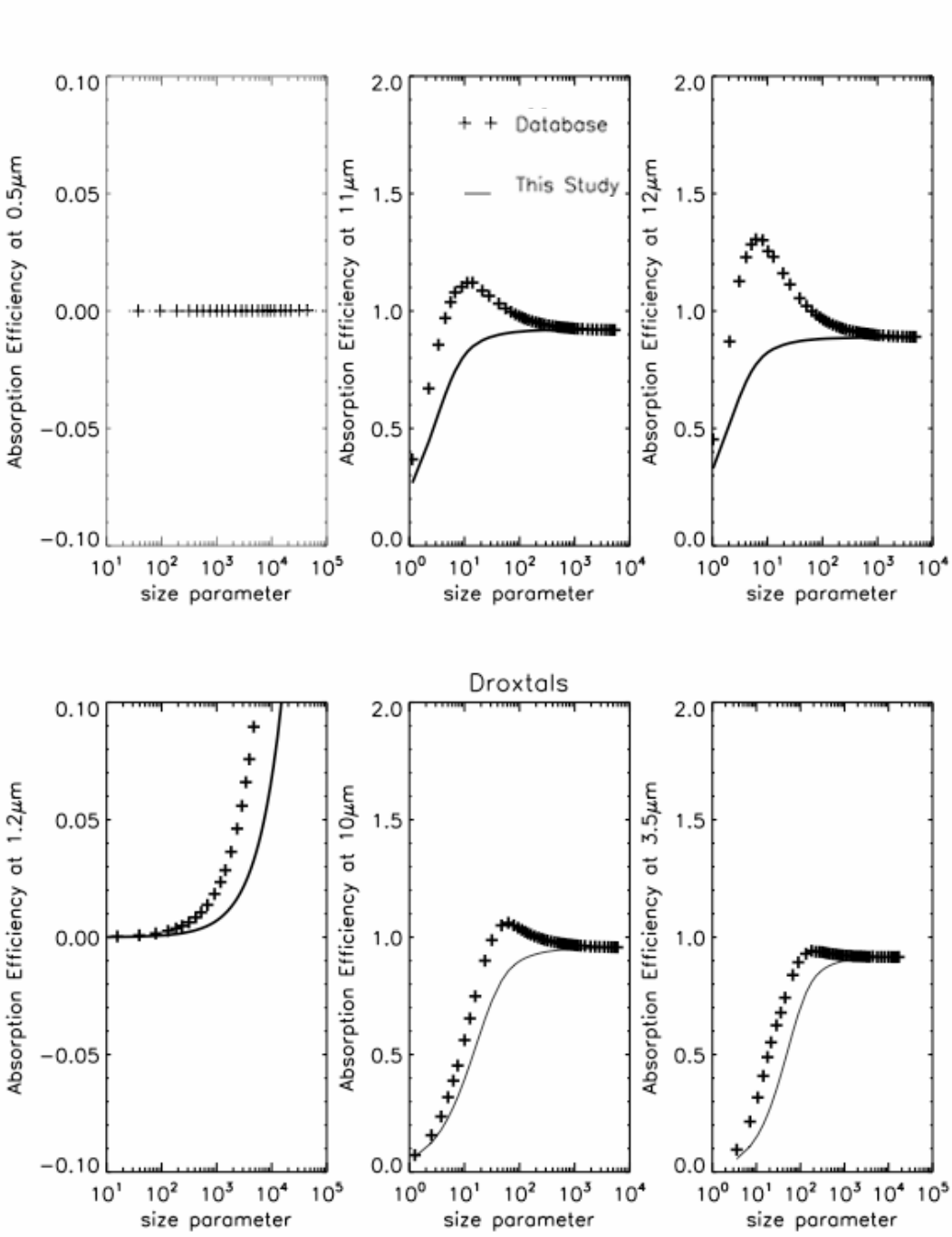

Figure 16 Absorption efficiencies of droxtals calculated using ray-by-ray method with the assumptions of ADT-based (dashed lines) and from the database (solid lines). The definitions of the solid column shape can be found in Yang et al., 2005

between ADT-based and IGOM-based optical properties is under 15% when the size parameter is larger than 30. The differences are caused by the same reasons as the extinction efficiency about the inaccuracy at the traveling distances inside the particle mentioned in section 3.1, the absorption efficiency is underestimated in the ADT. In addition, according to the discussion of Mitchell (1999), tunneling, which refers to the absorption of grazing photons beyond the physical cross section of the particle should be main reason for the underestimation for the size parameter is around 10. Further studies may be needed to take the internal reflections and edge effects into the consideration.

3.3 Asymmetry factor

The phase function is calculated based on Eqs. (5) to (10). Substituting the phase functions into Eq. (11), we obtain the asymmetry factors for solid columns, plates, bullets, aggregates, hollow columns and droxtals, which are demonstrated in Figs. 17, 18, 19, 20, 21, and 22 respectively. In the IR region (10 μm, 11 μm, and 12 μm), the relative errors between the simulated and the reference asymmetry factors become smaller from 9.5% to 3.1% as the size parameter grows and are less than 5.0% at large size parameters. The difference between the simulated and the reference asymmetry factors in six non-spherical shapes range from 1.03% to 19.99% in the near-IR region (3.5 μm). The errors of the asymmetry factors based on the ADT from the reference ones based on IGOM are caused by the negligence of the refraction phase functions and these errors are especially significant in the solar region (0.5 μm, and 1.2μm). Future work of the asymmetry factors based on the ADT in the solar part (0.5 μm and 1.23 μm) is necessary.

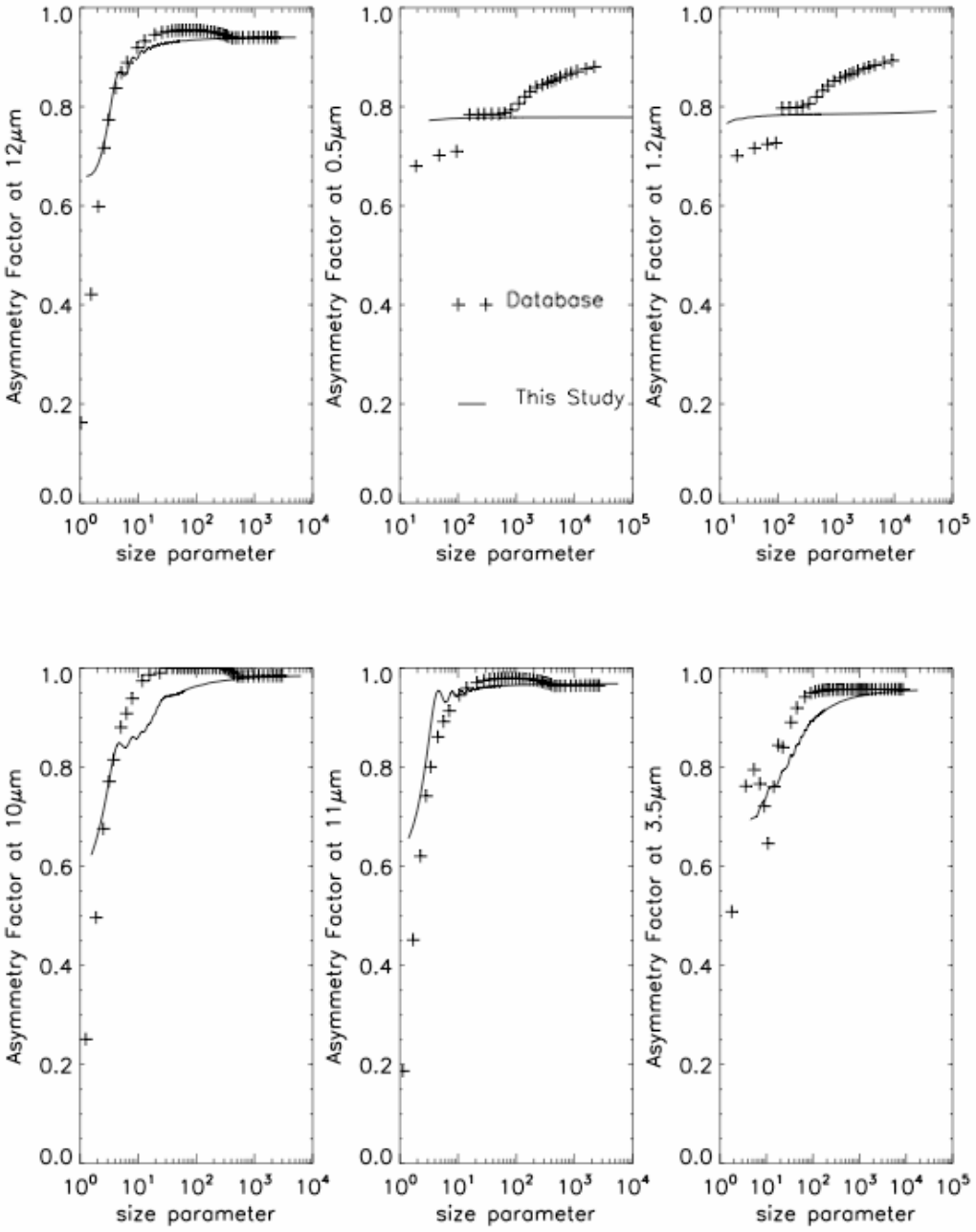

Figure 17 Asymmetry factors of solid columns calculated using ray-by-ray method with the assumptions of ADT-based (dashed lines) and from the database (solid lines). The definitions of the solid column shape can be found in Yang et al**.,** 2000

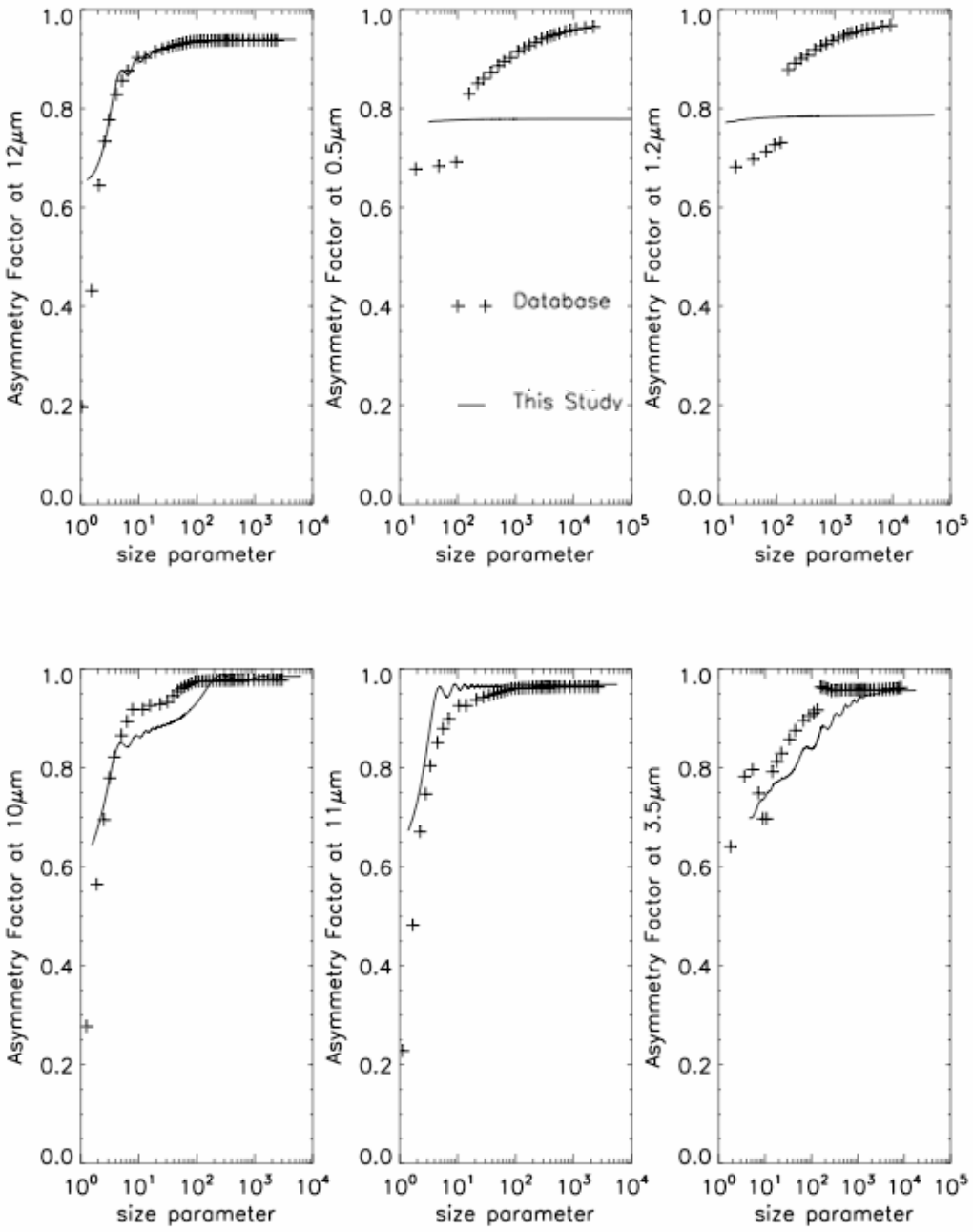

Figure 18 Asymmetry factors of plates calculated using ray-by-ray method with the assumptions of ADT-based (dashed lines) and from the database (solid lines). The definitions of the solid column shape can be found in Yang et al., 2000

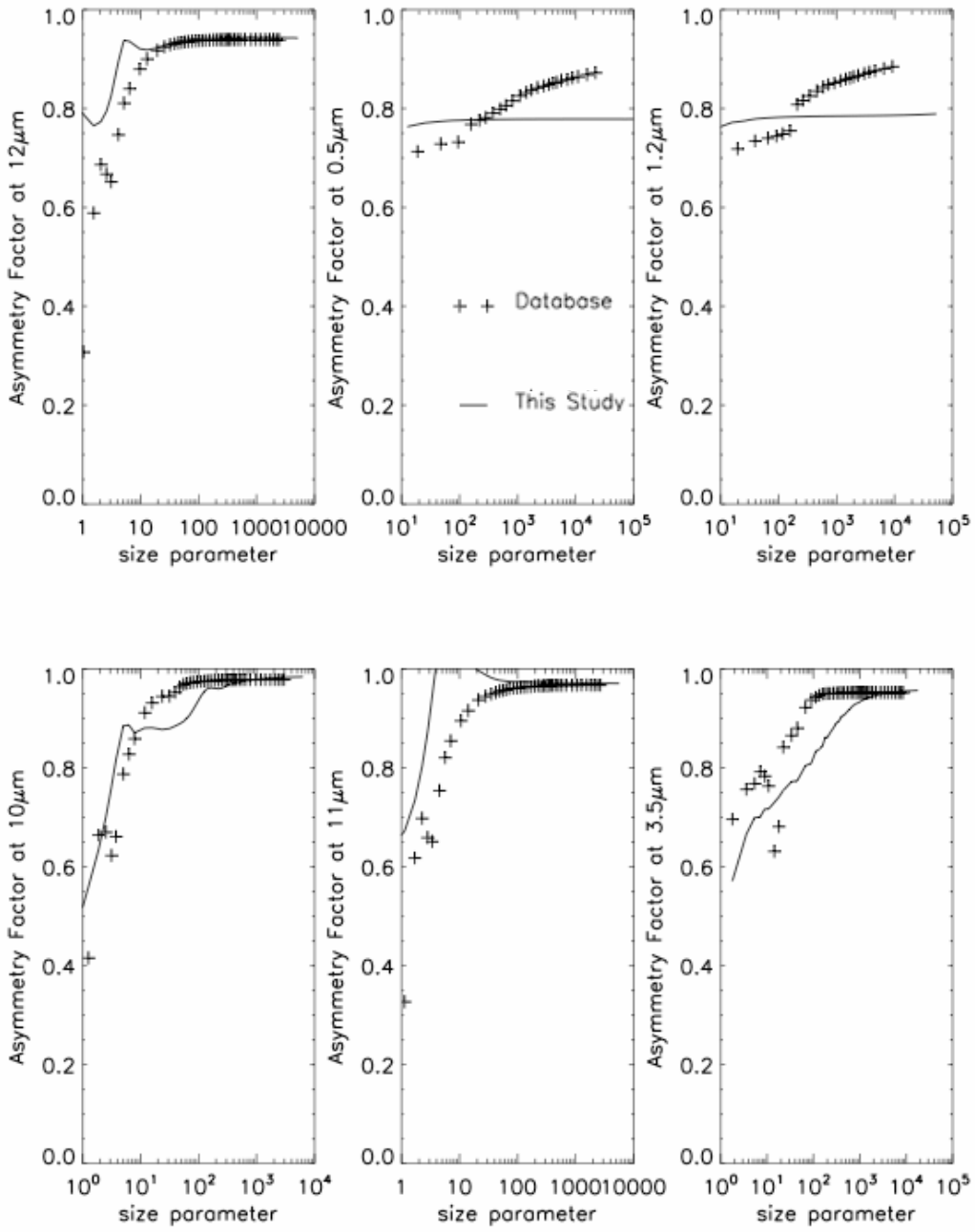

Figure 19 Asymmetry factors of bullet rosettes calculated using ray-by-ray method with the assumptions of ADT-based (dashed lines) and from the database (solid lines). The definitions of the solid column shape can be found in Yang et al., 2000

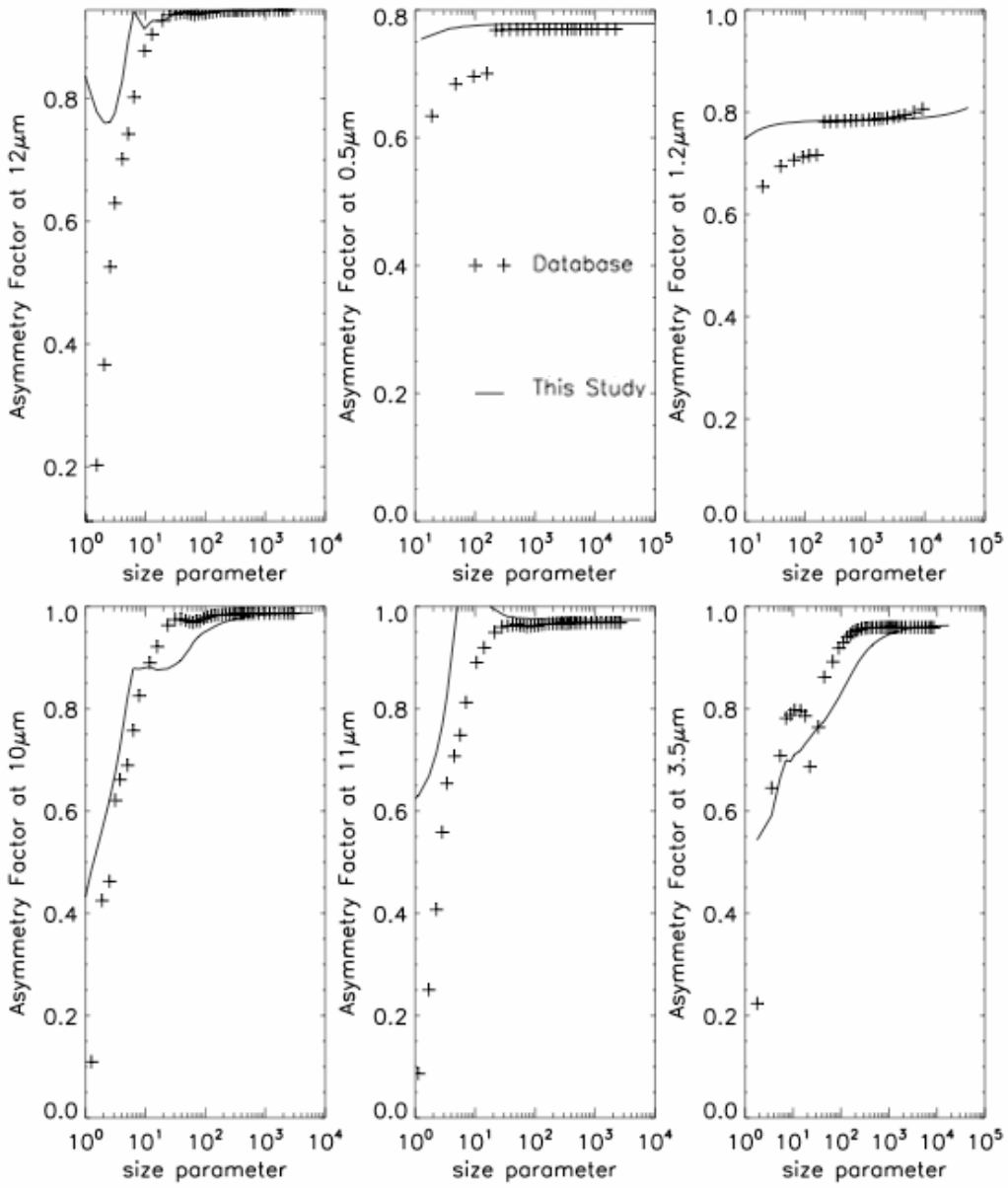

Figure 20 Asymmetry factors of aggregates calculated using ray-by-ray method with the assumptions of ADT-based (dashed lines) and from the database (solid lines). The definitions of the solid column shape can be found in Yang et al., 2000

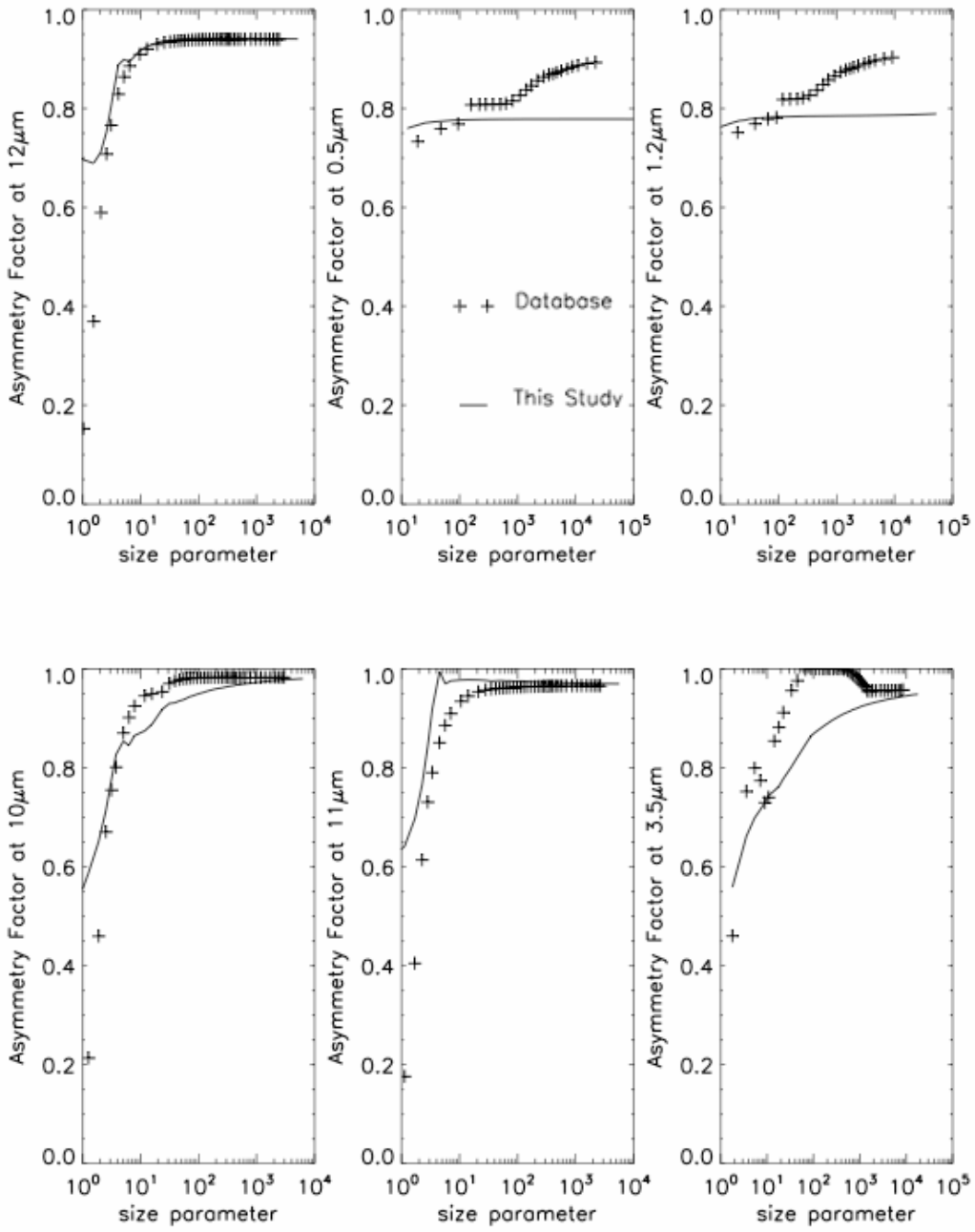

Figure 21 Asymmetry factors of hollow columns calculated using ray-by-ray method with the assumptions of ADT-based (dashed lines) and from the database (solid lines). The definitions of the solid column shape can be found in Yang et al., 2000

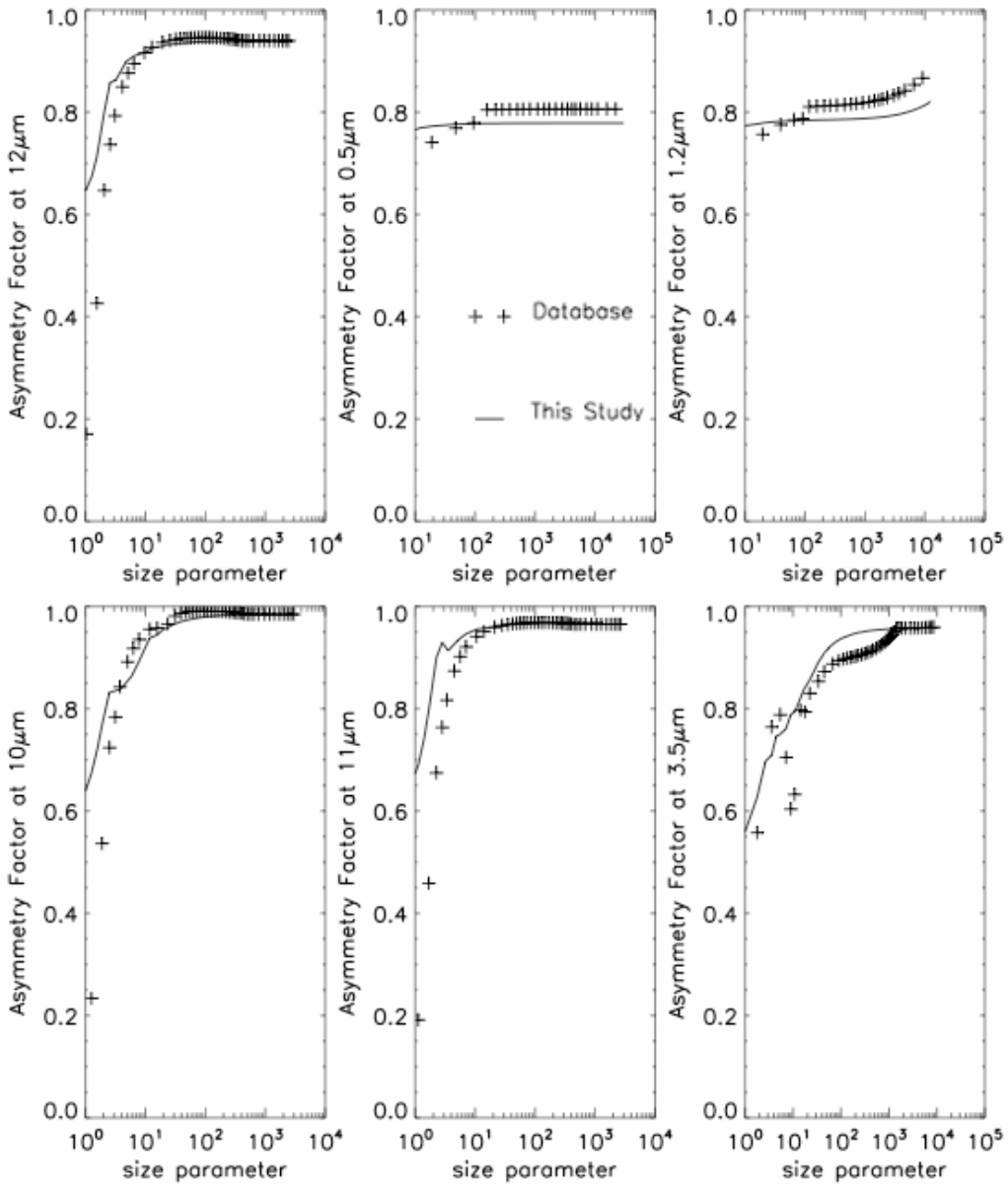

Figure 22 Asymmetry factors of droxtals calculated using ray by ray method with the assumptions of modified ADT (dashed lines) and from the database (solid lines). The definitions of the solid column shape can be found in Yang et al., 2005

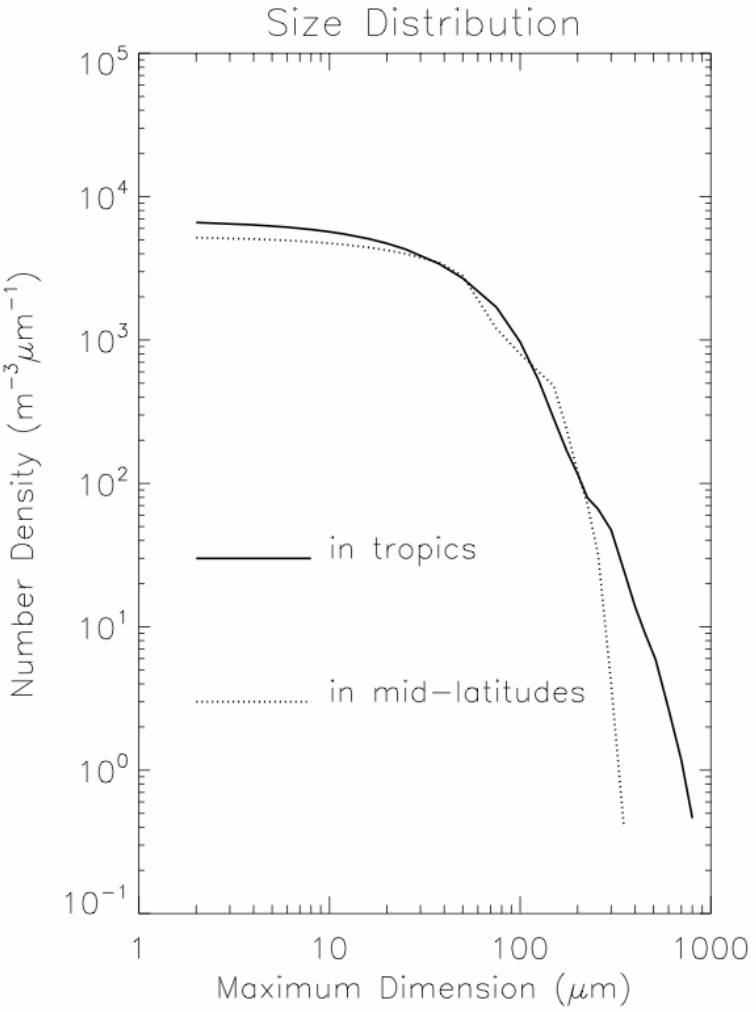

Figure 23 The two size distributions used in the study (Fu, 1996). The solid line represents the size distribution from tropics, the dashed line represents the size distribution from mid-latitude regions

Table 3 $f_h(D)$ function (Baum et al., 2005)

D is the maximum dimension of the particle

D < 60 microns:	100% droxtals
60 microns < D < 1000 microns:	15% 3D bullet rosettes 50% solid columns 35% plates
1000 microns < D < 2500 microns	45% hollow columns 45% solid columns 10% aggregates
2500 microns < D < 9500 microns	97% 3D bullet rosettes 3% aggregates

3.4 Bulk optical properties

Once the single-scattering properties of ice particles in six different shapes are obtained, it is straightforward to calculate the bulk optical properties according to Baum et al. (2005).

The band-weighted mean extinction cross section can be expressed as

$$\overline{\sigma}_{ext} = \frac{\int_{\lambda_1}^{\lambda_2}\int_{D_{\min}}^{D_{\max}}[\sum_{h=1}^{6}\sigma_{ext,h}(D,\lambda)\,f_h(D)]n(D)S(\lambda)dDd\lambda}{\int_{\lambda_1}^{\lambda_2}\int_{D_{\min}}^{D_{\max}}[\sum_{h=1}^{6}f_h(D)]n(D)S(\lambda)dDd\lambda} \qquad (12)$$

where $f_h(D)$ is the ice particle habit fraction for the habit h (Baum et al., 2005) and Table 3 gives the detail of this function. D is the maximum dimension of the particle, λ is wavelength, S(λ) is the solar spectrum or the Plank function, and n(D) is the number density of ice crystals in cirrus clouds. Figure 23 shows the particle size distributions used in this study. These particle size distributions are chosen from the observation data and used in Fu (1996). The size distribution from the tropical region has more large ice particles than that from the mid-latitude region. This might be due to the fact that the convections are stronger and the absolute humidity tends to be higher in the tropics.

Similarly, the band-weighted mean scattering cross section is given by

$$\overline{\sigma}_{sca} = \frac{\int_{\lambda_1}^{\lambda_2}\int_{D_{\min}}^{D_{\max}}[\sum_{h=1}^{M}\sigma_{sca,h}(D,\lambda)\,f_h(D)]n(D)S(\lambda)dDd\lambda}{\int_{\lambda_1}^{\lambda_2}\int_{D_{\min}}^{D_{\max}}[\sum_{h=1}^{M}f_h(D)]n(D)S(\lambda)dDd\lambda}\quad , \qquad (13)$$

and the single-scattering albedo can be expressed as

$$\overline{\omega} = \frac{\overline{\sigma_{sca}}}{\overline{\sigma_{ext}}}. \tag{14}$$

The band-averaged asymmetry factor is calculated according to the following equation:

$$\overline{g} = \frac{\int_{\lambda_1}^{\lambda_2}\int_{D_{\min}}^{D_{\max}}[\sum_{h=1}^{M} g_h(D,\lambda)\sigma_{sca,h}(D,\lambda) f_h(D)]n(D)S(\lambda)dDd\lambda}{\int_{\lambda_1}^{\lambda_2}\int_{D_{\min}}^{D_{\max}}[\sum_{h=1}^{M} \sigma_{sca,h}(D,\lambda) f_h(D)]n(D)S(\lambda)dDd\lambda}. \tag{15}$$

The effective size of the size distribution is given as

$$\overline{D}_{eff} = \frac{3}{2}\frac{\sum_{h=1}^{M}\int_{D_{\min}}^{D_{\max}}[V_h(D)n(D)dD]}{\sum_{h=1}^{M}\int_{D_{\min}}^{D_{\max}}[A_h(D)n(D)dD]} \tag{16}$$

Based on Eqs.(12) to (15), the bulk optical properties are calculated and shown in Figs. 24 and 25. The errors of the bulk extinction properties in the 18 bands between the ADT-based and the IGOM data are small, under 1.89%. It is because the simulated extinction efficiencies of six non-spherical ice particles always match very well with the reference. Errors of the bulk absorption properties between ADT and IGOM are small in the first 6 solar bands of Fu-Liou model, but a relatively large underestimation is noticed in the 7-18 bands that are in the IR regions. This result is consistent with the underestimations of individual absorption efficiency based on ADT in the IR. The good agreement of bulk extinction efficiency and the underestimation of the bulk absorption efficiency indicate that a poor agreement of the bulk scattering efficiency. Therefore, ADT assumptions may give rise to substantial errors in computing the scattering and absorption effects. The bulk asymmetry factors are underestimated in all the 18 bands and relative errors are 20%-30%.

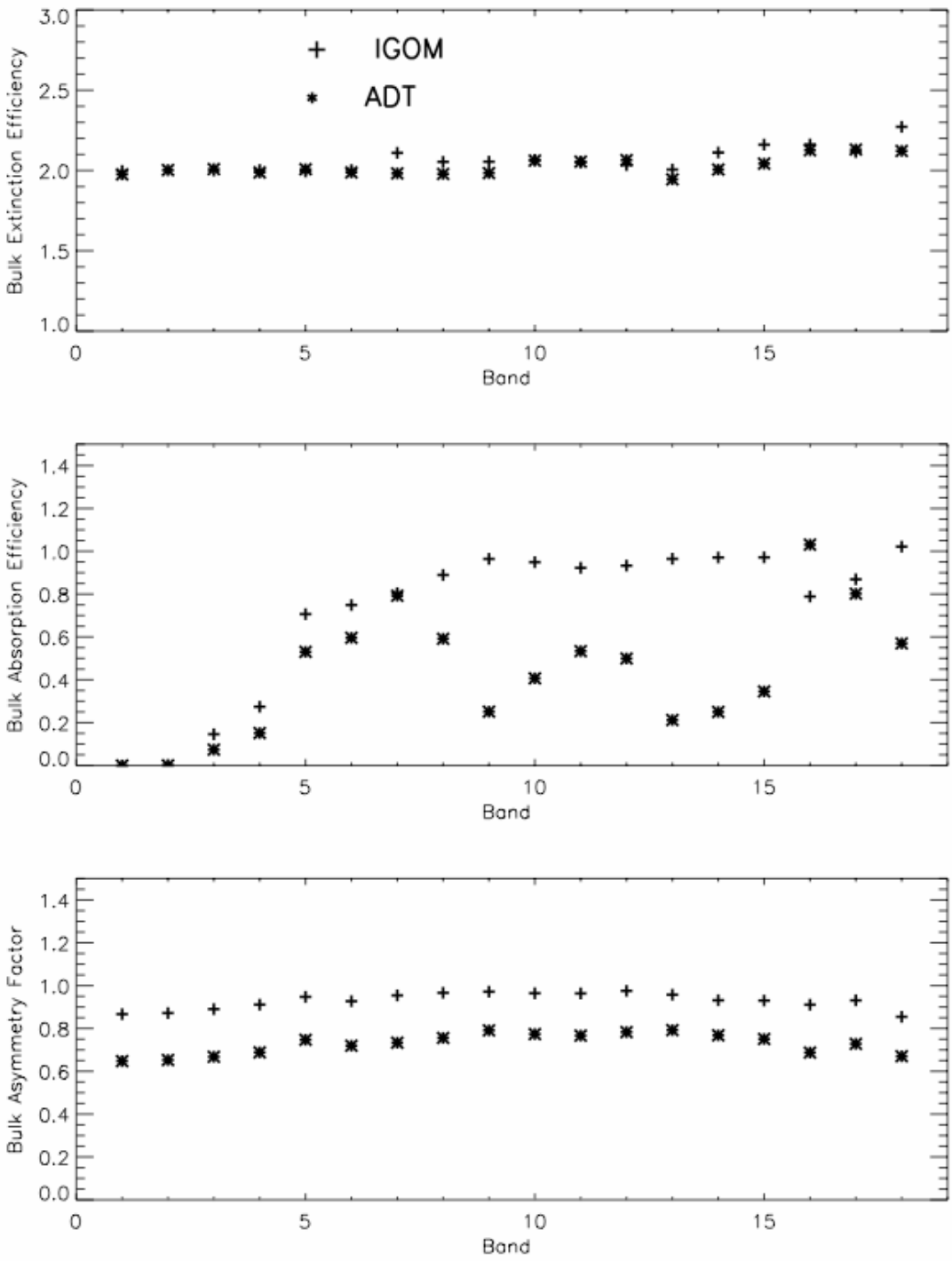

Figure 24 The bulk optical properties with the tropical size distribution (the plus signs '+' are from the reference database (IGOM), and the asterisks '*' are from the ADT-based data): the top panel illustrates the bulk extinction efficiency of 18 bands in the Fu-Liou model; the middle panel illustrates the bulk absorption efficiency; the bottom panel illustrates the bulk asymmetry factor

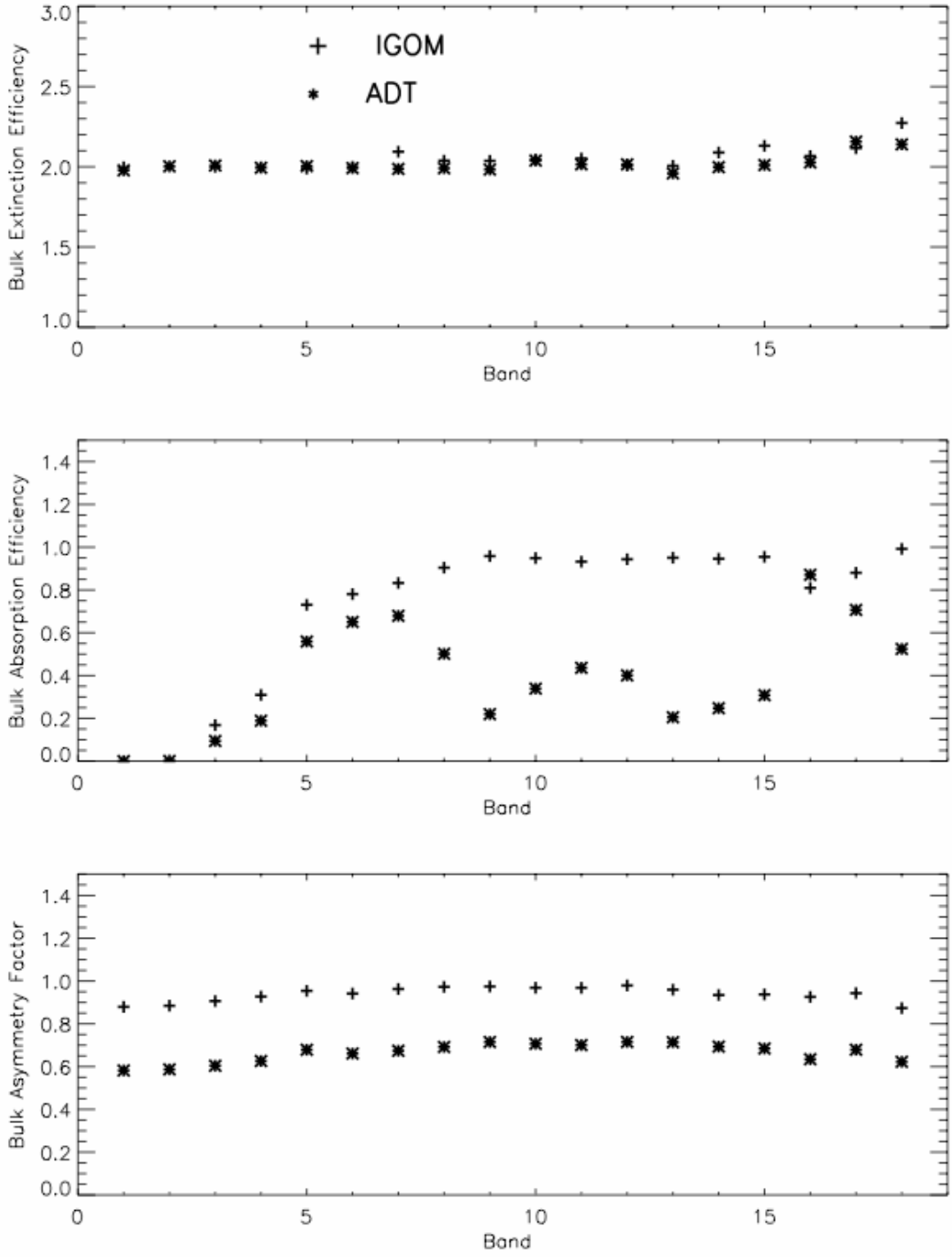

Figure 25 Same as Figure 24 except for the bulk optical properties with the mid-latitude size distribution

4. RADIATIVE FLUX CALCULATION

4.1 The model description and initialization

The simulated bulk optical properties from the modified ADT are introduced into the Fu-Liou model to calculate the radiative fluxes and the heating rates and compared with the radiative properties from the reference IGOM optical properties. To make the parameterization of the radiative properties of cirrus clouds reliable, two cases are designed for the study in this thesis: one for the tropics and the other for the mid-latitudes. In the radiative simulation, particle size distribution, and profiles associated with the ozone mixing ratio, water vapor mixing ratio, and temperature are required. For the tropical case, a size distribution with the observed effective size of 116.86 μm is employed, and three aforementioned profiles are obtained from American tropical standard atmospheric profile; as for the case simulating cirrus clouds in the mid-latitude districts, we use a size distribution with the effective size of 140.99 μm from the observation, and three aforementioned profiles from the U.S. standard atmospheric profile for the mid-latitudes. Both two ice crystal size distributions are shown in Fig. 23, which have been used by Fu (1996) to study the radiative properties of cirrus clouds for climate models. Atmospheric profiles for two cases are illustrated in Fig. 26.

The surface temperature is assumed to be 300 K for the tropical case, and 288 K for the mid-latitude case. The IR surface emissivity is assumed to be 1 and the solar surface albedo is set to be 0.07. In the atmosphere, the only clouds are cirrus clouds. The cloud heights are from the zonal averaged cloud heights in the northern hemisphere (Liou 1986). The cloud top height for the tropical case is 11 km, whereas the mid-latitude cirrus cloud top height is 10 km. The cloud thickness is 1 km. In both cases, the model uses

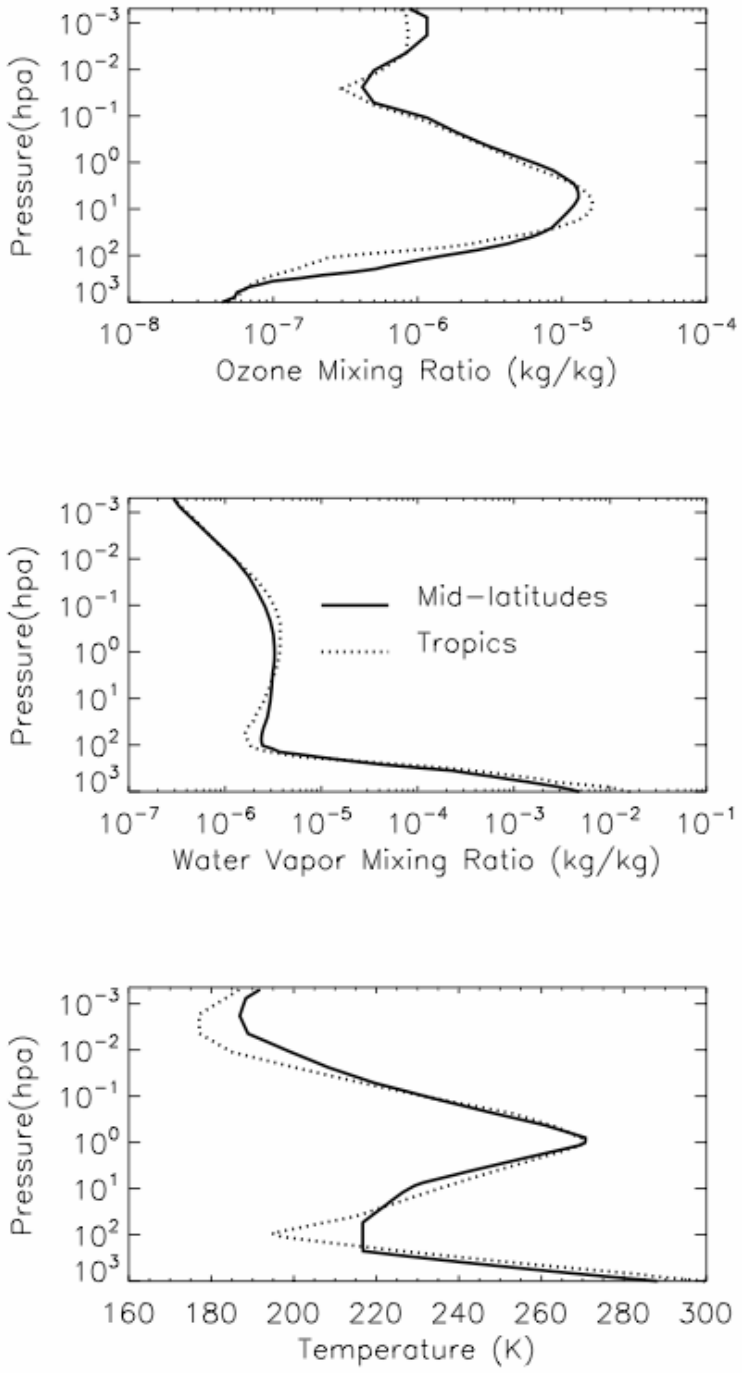

Figure 26 Temperature profiles, water vapor mixing ratio profiles and ozone mixing ratio profiles from American tropical and mid-latitude standard atmospheric profiles

four-stream approximation. There are 35 layers in the Fu-Liou model (layer 1 is TOA and layer 35 is surface). Optical depths at 0.55 μm are used to control the optical depth of cirrus clouds in the Fu-Liou model and they are set from 0.1 to 100. The cosines of solar zenith angle range from 0.1 to 1.

4.2 Upward IR fluxes and downward IR fluxes

Figures 27 and 28 illustrate the upward and downward IR fluxes for tropical cirrus clouds which are in function of optical depth. Figures 27a,d and 28a,d are based on the reference optical properties from IGOM; Figures 27b,e and 28b,e are based on the optical properties from ADT; Figures 27c,f and 28c,f show the relative difference. It is evident that there are no differences for the upward IR fluxes below the cirrus clouds, and for the downward IR fluxes above the cirrus clouds. From Figs. 27a, 27b, 28a and 28b, it is shown that the upward IR fluxes above the clouds regress significantly when the optical depth of cirrus clouds at 0.55 μm ($\tau_{0.55}$) increases from 0 to 4, but almost do not change when $\tau_{0.55}$ is larger than 4. In addition, Figs. 27d, 27e, 28d and 28e show that the downward IR fluxes below the clouds endure significant increases before $\tau_{0.55}$ reaches 4 and remain their values after that. The regression of upward IR fluxes and the degression of downward IR fluxes are caused by the strong absorptive ability of ice crystals. When $\tau_{0.55}$ reaches about 20, the cirrus cloud can be treated as black body to IR fluxes. Figures 27c and 28c show the relative errors of upward IR fluxes with the simulated and reference optical properties. It is evident that the upward IR fluxes are underestimated when using the simulated optical properties. The relative errors reach the minimum value

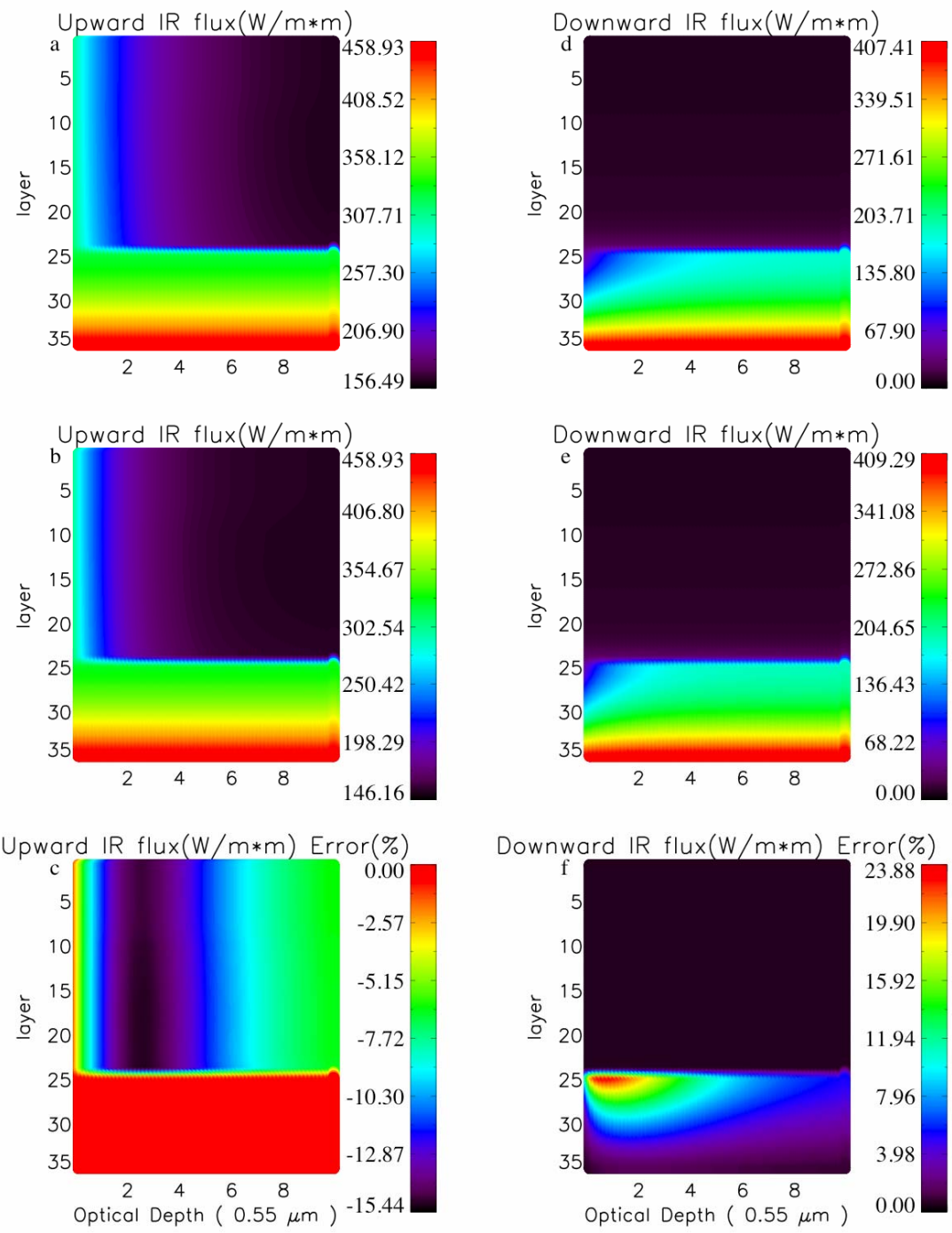

Figure 27 (a) and (d) Upward and downward IR flux from the reference IGOM data with the size distribution at tropics when the range of the optical depth (0.55 μm) is from 0.1 to 10; (b) and (e) upward and downward IR flux from the ADT-based method; (c) and (f) relative errors between the ADT-based method and the IGOM-based data

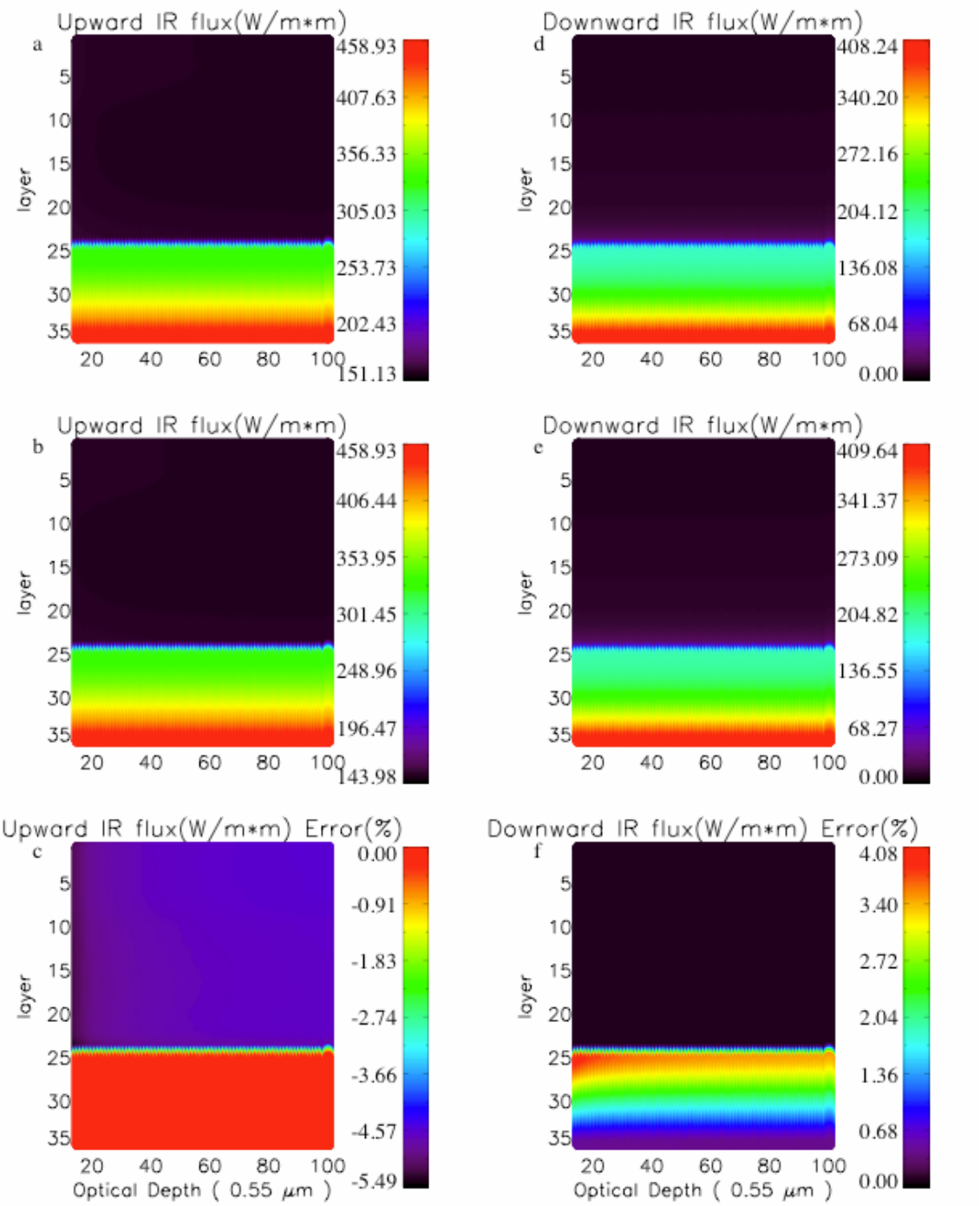

Figure 28 Same as Figure 27 except that the range of the optical depth (0.55 m) is from 10 to 100 and the size distribution is in the tropical regions

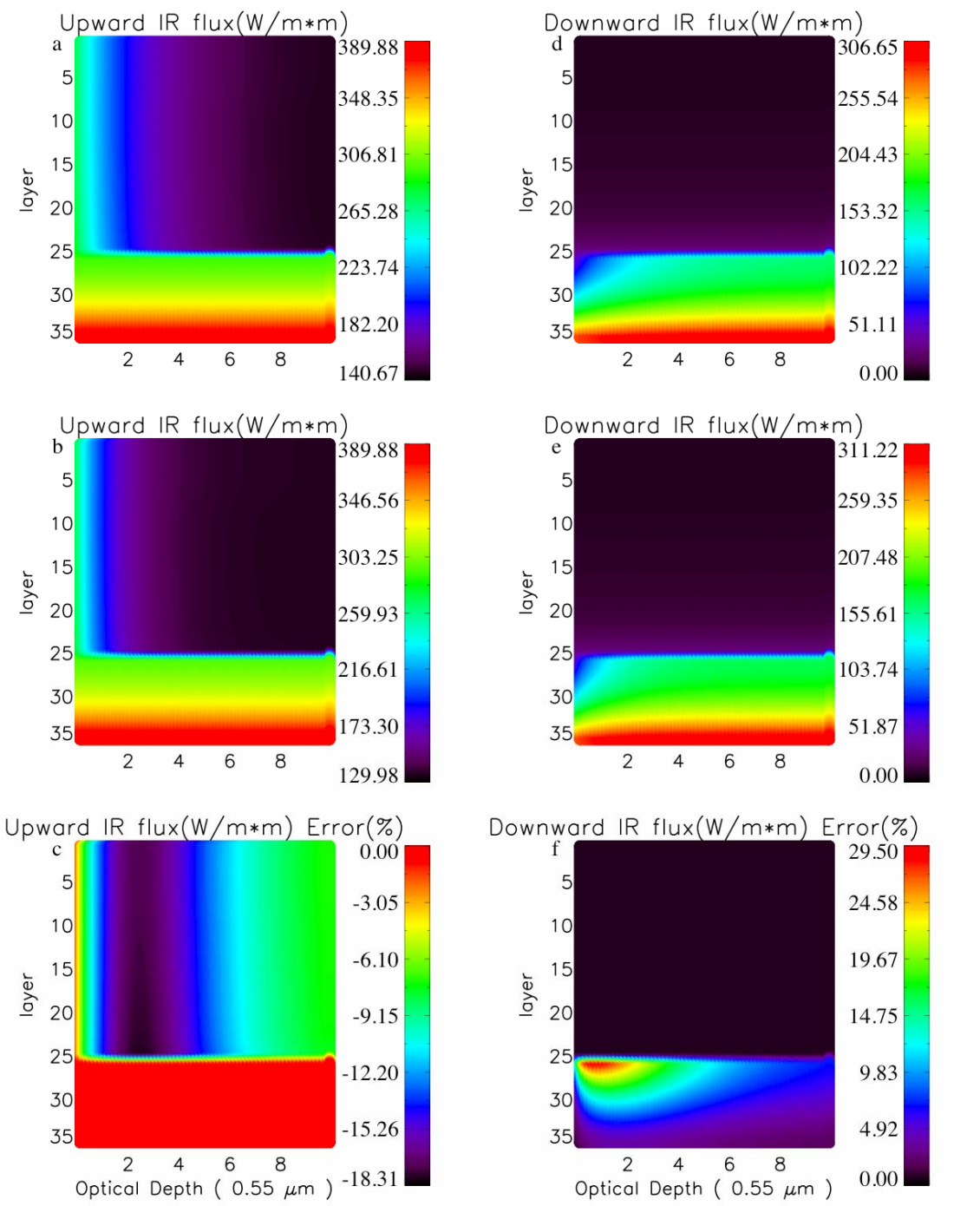

Figure 29 Same as Figure 27 except that the range of the optical depth (0.55 m) is from 0.1 to 10 and the size distribution is in the mid-latitude regions

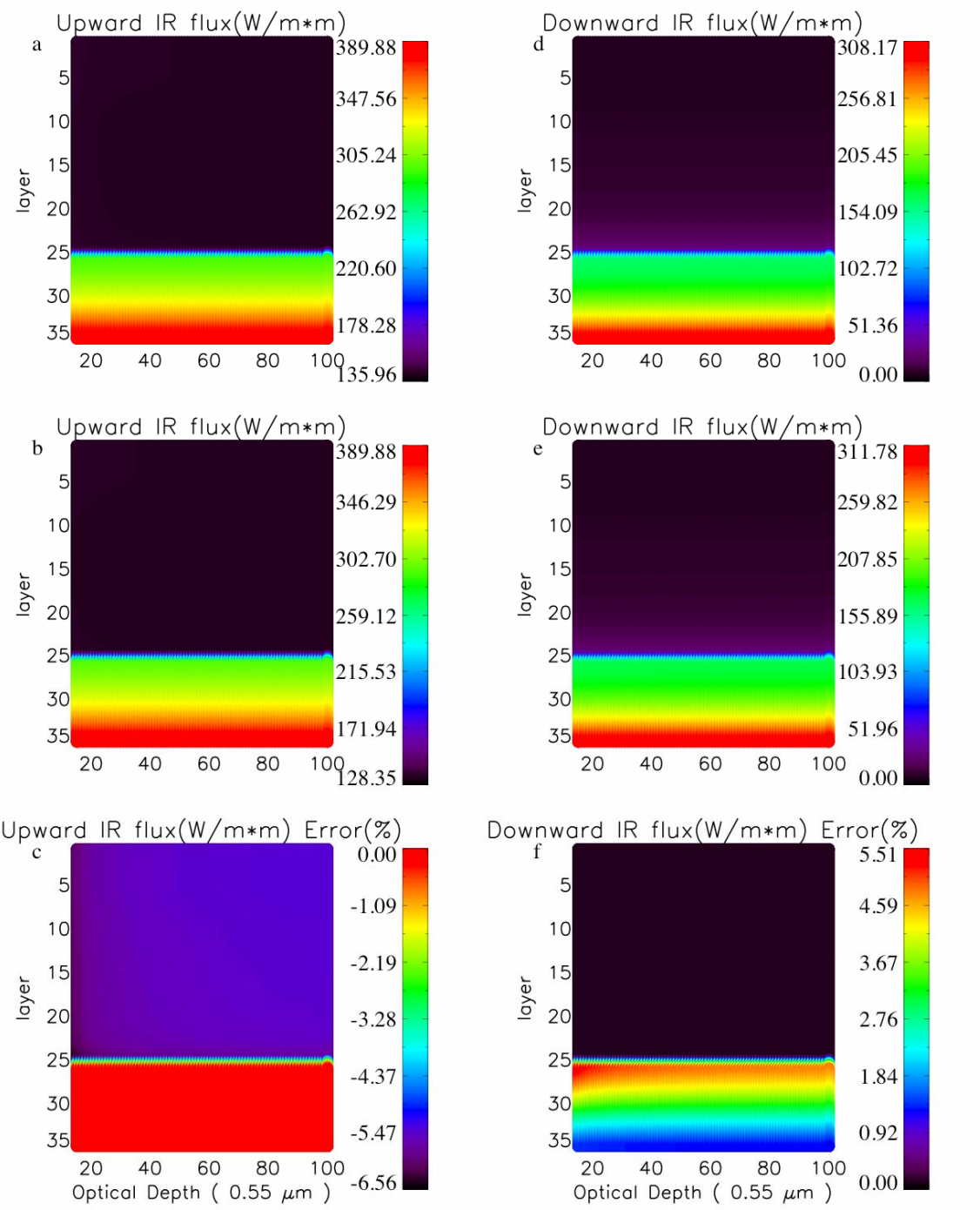

Figure 30 Same as Figure 27 except that the optical depth (0.55 m) is from 10 to 100 and the size distribution is in the mid-latitude regions

-15.44% when $\tau_{0.55}$ is about 2.3 and induce to about -4.08% as $\tau_{0.55}$ increases. Figures 27f and 28f indicate the relative errors of downward IR fluxes with both the simulated and reference optical properties. The downward IR fluxes are overestimated with the simulated optical properties. In the layer just below the cirrus clouds, the downward IR fluxes relative errors increase to 23.88% when $\tau_{0.55}$ is near 1 and decrease the values to 4.08% when $\tau_{0.55}$ grows to about 20. The trends of the relative errors of upward and downward IR fluxes can be explained as the combined effects from the errors of the bulk absorption efficiency and the bulk asymmetry factor. The bulk absorption efficiency in the IR region is underestimated and the upward IR fluxes are underestimated and the downward fluxes are overestimated. The underestimation of the bulk asymmetry factor can generate more backward flux and thus exaggerate the relative errors of upward and downward IR when the cirrus clouds are optically transparent in the IR region. Also, in Fig. 28f, it is noted that the relative errors of downward IR fluxes increase from 0.5% to 4.08% when the layer goes up from surface to the cirrus clouds, but in Fig. 28c, the upward IR flux errors remain -4.0%.

Figures 29 and 30 show the upward IR fluxes, downward IR fluxes based on two sets of ice optical properties and their relative errors for the mid-latitude cirrus clouds. Consistent with Figs 27 and 28, a minimum of relative errors for the underestimated upward IR fluxes is -18.31%, which appends at $\tau_{0.55}$ is about section 2.3 and a maximum of relative errors for the overestimated downward IR fluxes is 29.5% when $\tau_{0.55}$ reaches 1. Moreover, when $\tau_{0.55}$ goes larger than 20, similarly with the results in Figs 27 and 28, the relative differences of the upward IR fluxes based on two sets of optical properties above the cirrus clouds go to -5.5%, and the relative difference for downward IR fluxes reaches

to 5.5% below the cloud and 0.92% at surface. Although the relative differences for the IR fluxes can reach relative large values to 29.5% at the layers near the cloud, it is noted that relative differences of upward IR fluxes at TOA and downward IR fluxes at surface, the fluxes which possess practical meanings, are low. For cirrus clouds in tropics and mid-latitudes, upward IR fluxes at TOA have relative differences about -4.0%; the relative errors of downward IR fluxes at surface with two sets of optical properties are always less than 4.0%. Thus we can conclude that the ADT-based optical properties can generate reasonable IR fluxes for the practical use.

Comparing Figs. 29 with 27 and Figs. 28 with 26, upward and downward IR fluxes of the tropical cirrus clouds have generally smaller relative errors than those of the mid-latitude cirrus clouds. These can be explained that the bulk optical properties associated with the tropical cirrus clouds have lower relative errors than those associated with the mid-latitude case.

4.3 Upward solar fluxes and downward solar fluxes

Figures 31 and 32 are the same as Figs. 27 and 28, but for the upward and downward solar fluxes. The cosine of solar zenith angle is 0.1. The relative difference of upward solar fluxes in the entire atmosphere in function of $\tau_{0.55}$ between the two sets of optical properties is shown in Figs. 31c and 32c. The upward solar fluxes from ADT-based optical properties have larger values than those from the IGOM-based data. The relative errors of upward solar fluxes increase when the layer rises from the cloud top to the TOA. Moreover, the upward solar flux errors are sensitive to $\tau_{0.55}$. For example, at

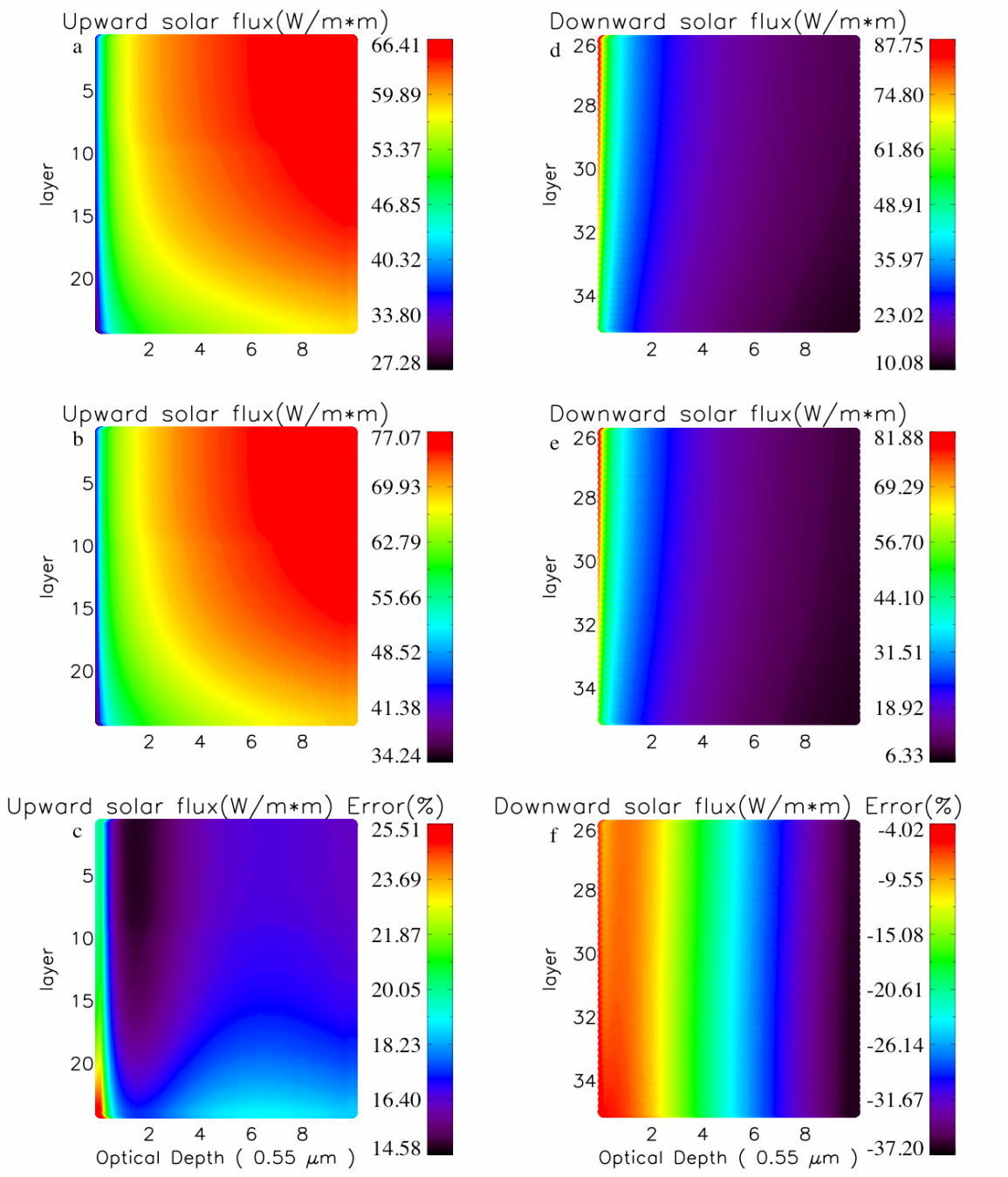

Figure 31 (a) and (d) Upward and downward solar flux in function of layers and optical depths (0.55 μm) from the reference IGOM data with the size distribution at tropics when the range of the optical depth (0.55 μm) is from 0.1 to 10 and the cosine of solar zenith angle is 0.1; (b) and (e) upward and downward IR flux from the ADT-based method; (c) and (f) relative errors between the ADT-based and the reference data

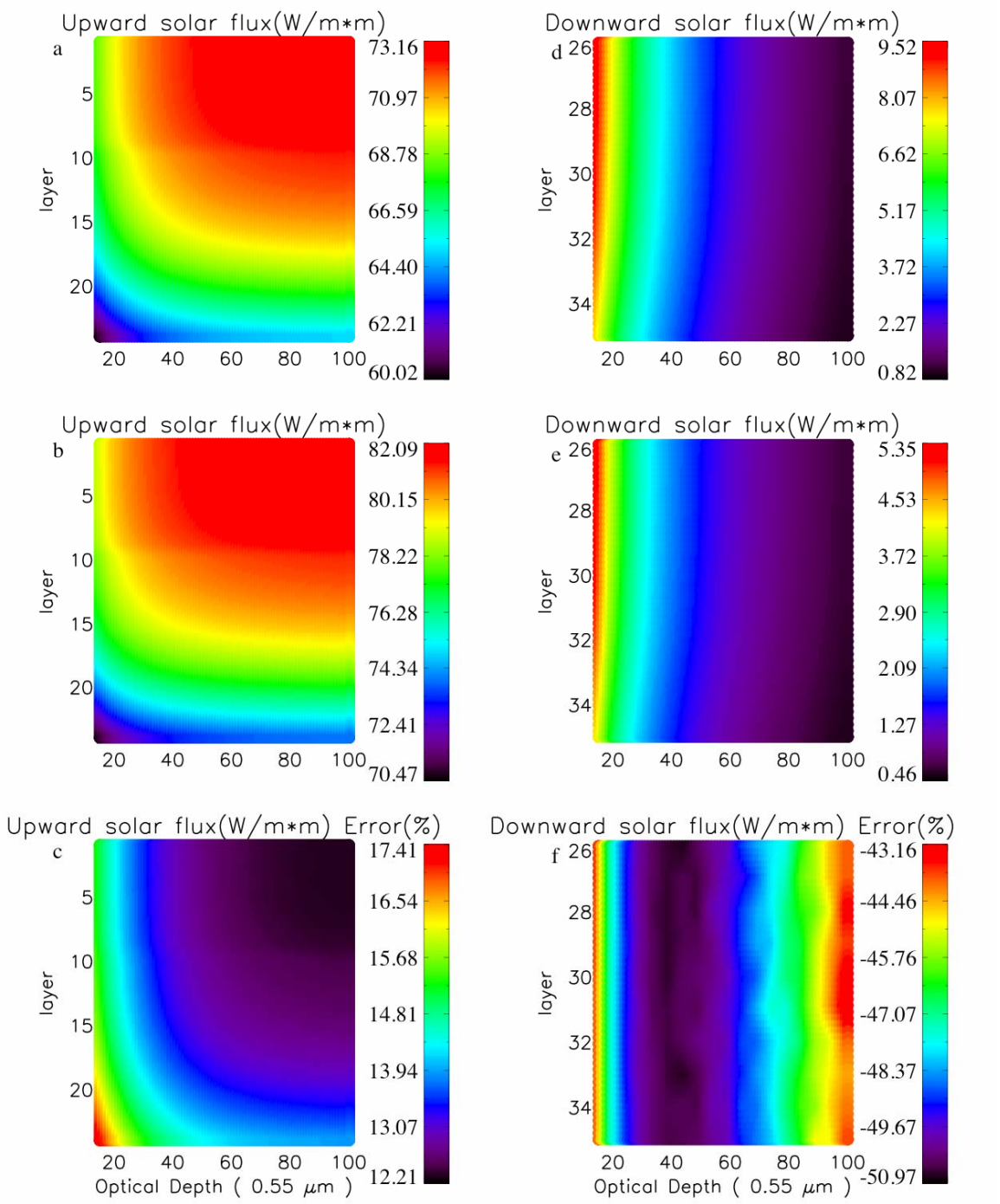

Figure 32 Same as Figure 31 except that the range of the optical depth (0.55 m) is from 10 to 100 the size distribution in the tropical regions

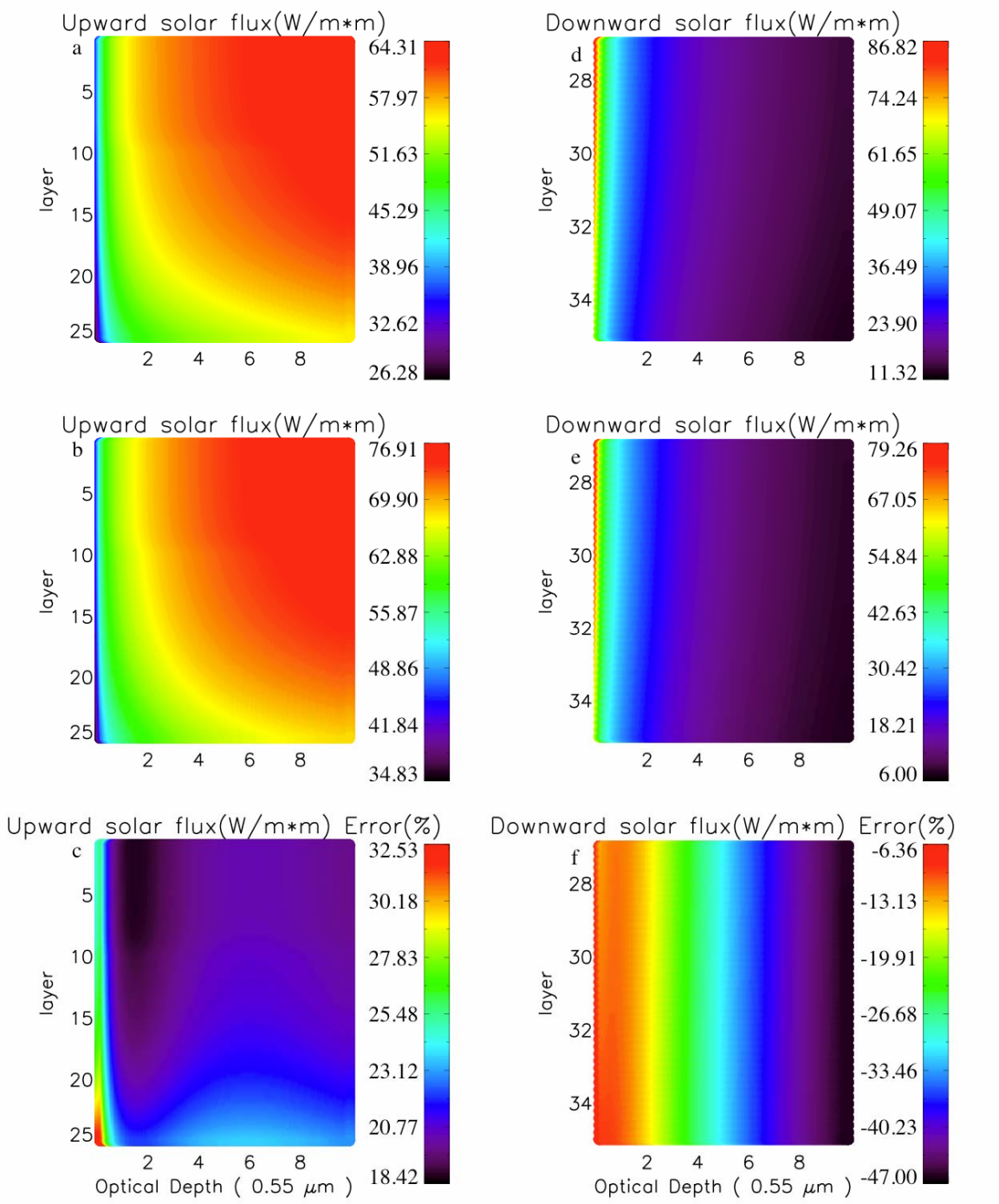

Figure 33 Same as Figure 31 except that the range of the optical depth (0.55 m) is from 0.1 to 10 and the size distribution is in the mid-latitude regions

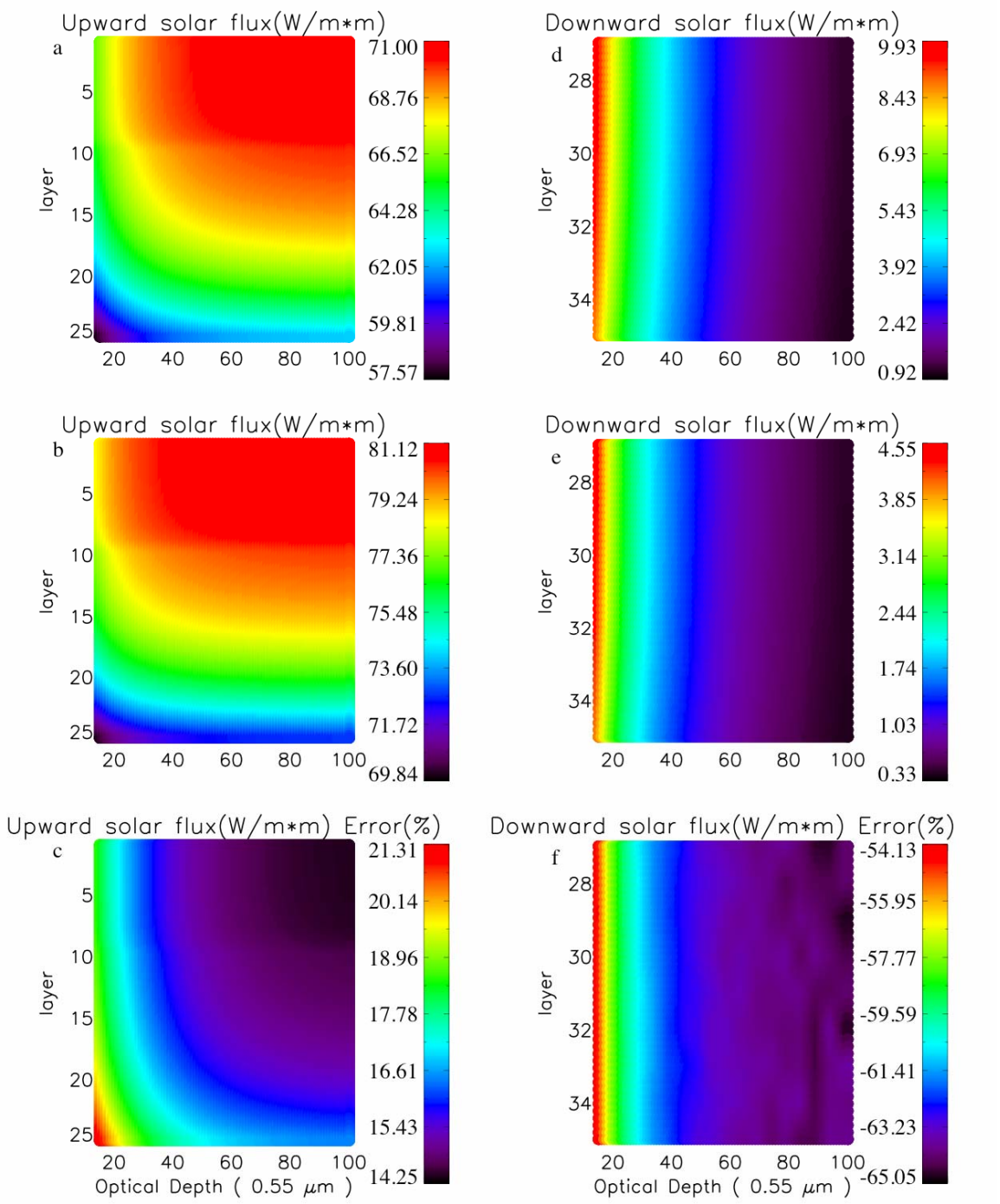

Figure 34 Same as Figure 31 except that the size distribution is in the mid-latitude regions and the range of the optical depth (0.55 m) is from 10 to 100

TOA, the relative errors of upward solar fluxes decrease from 0.1 to 1.5 and increase from the minimum 14.58% to 17.41% afterwards. Figures 31f and 32f illustrate the relative differences of downward solar fluxes between the two optical properties. The reduction of downward solar fluxes increases from 6.36% to 65.05% when $\tau_{0.55}$ changes from 0.1 to 100. Fig. 33 and Fig. 34 are the same as Fig. 31 and Fig. 32 except for the mid-latitude case. The upward solar flux errors in Figs. 33c and 34c are larger than those in Fig. 31c and Fig. 32c and the downward solar flux in Figs. 33f and 34f also underestimate more comparing than those in Figs. 31f and 32f.

Upward and downward solar fluxes are also the function of solar zenith angles. Figs. 35 and 36 shows upward solar fluxes at TOA and downward solar fluxes at surface for the tropical cirrus clouds using the simulated and reference optical properties with cosine of solar zenith angle is 0.1. The relative errors of upward solar fluxes shown in Figs. 35c and 36c become larger as cosine of solar zenith angle increases. In addition, there is one interesting result we should notice. In Fig. 35c, there is an obvious maximum value of relative upward solar flux errors when $\tau_{0.55}$ is about 4 and cosine of zenith angle is 1. However, in Fig. 31c, the relative error of upward fluxes at TOA reaches minimum when $\tau_{0.55}$ is about 1.5. In short, as $\tau_{0.55}$ is from 0.1 to 4, the relative errors of upward solar fluxes will have a minimum value when cosine of solar zenith angle is 0.1 and when cosine of solar zenith angle is larger, the relative errors will become a maximum value instead. Figs. 35f and 36f indicate that the downward solar fluxes are underestimated using the simulated optical properties; the underestimation grows with the increase of optical depth. Optical depth also influences the effects of solar zenith angle on the relative errors of downward solar fluxes. When $\tau_{0.55}$ is smaller than 2, the relative errors

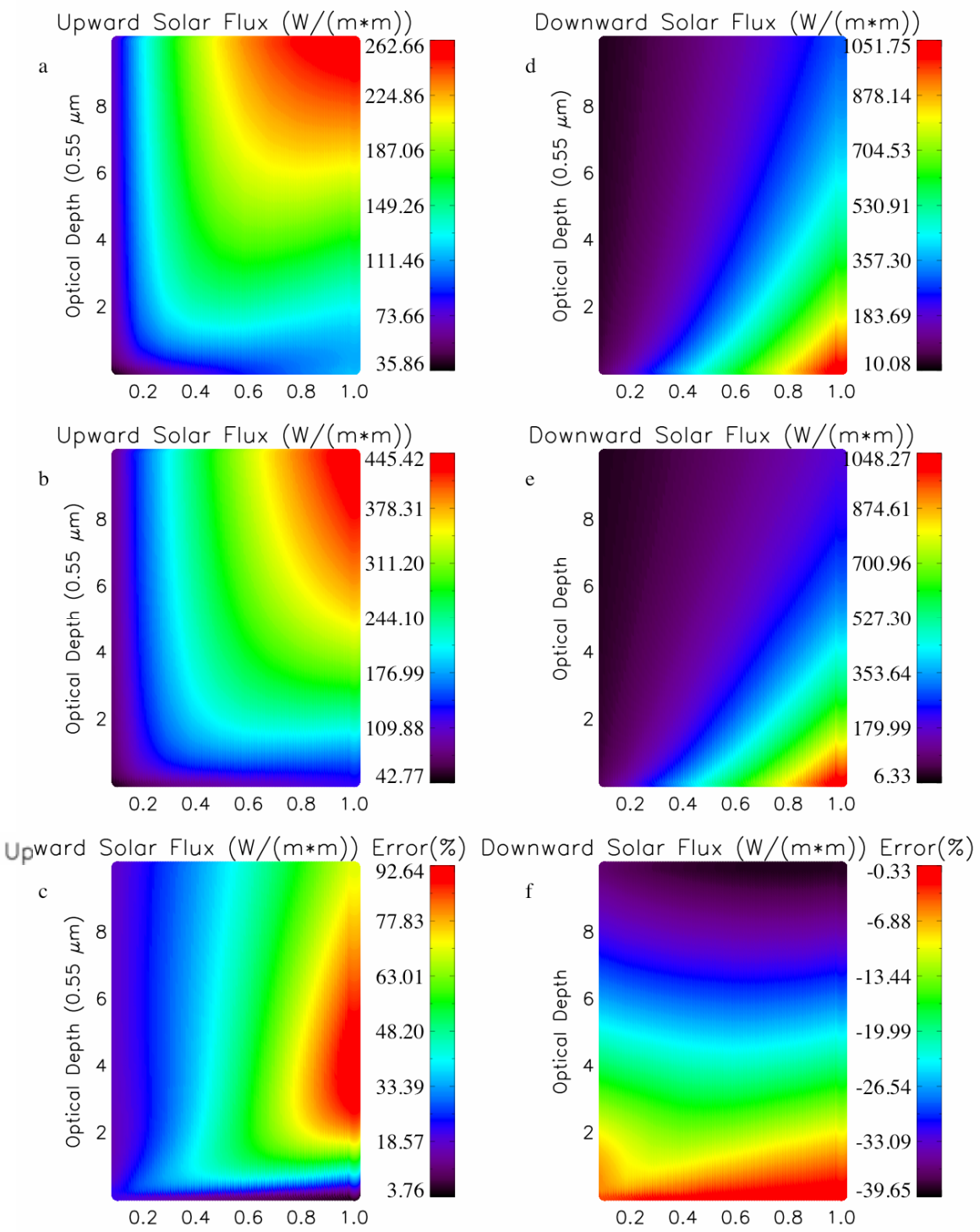

Figure 35 (a) and (d) Upward solar flux at TOA and downward solar flux at surface in function of optical depths (0.55 μm) from the IGOM-based data with the size distribution at tropics when the range of the optical depth (0.55 μm) is from 0.1 to 10; (b) and (e) upward and downward solar fluxes from the ADT-based method; (c) and (f) relative errors between the ADT-based and the IGOM-based data

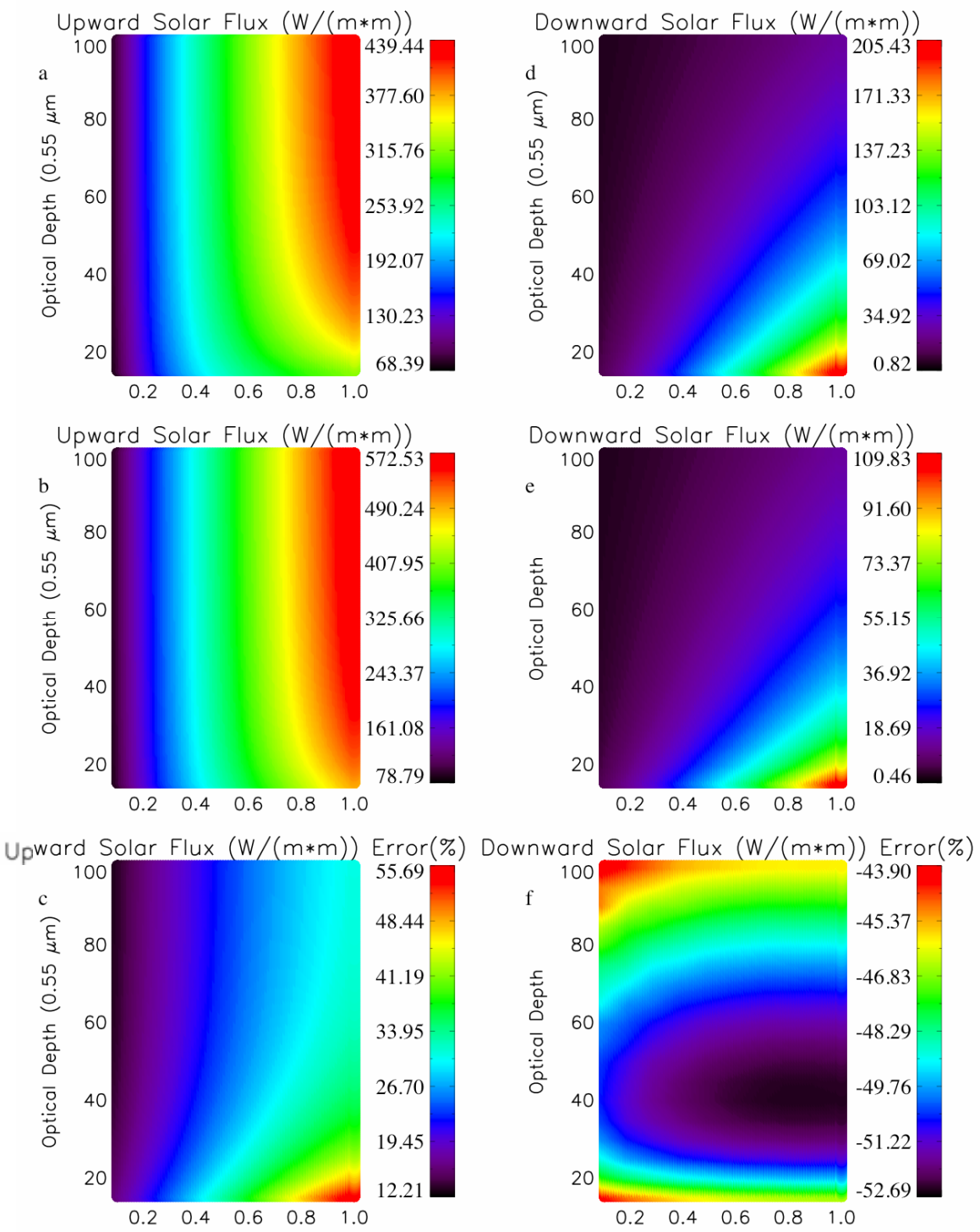

Figure 36 Same as Figure 35 except that the size distribution is in the tropical regions and the range of the optical depth (0.55 m) is from 10 to 100

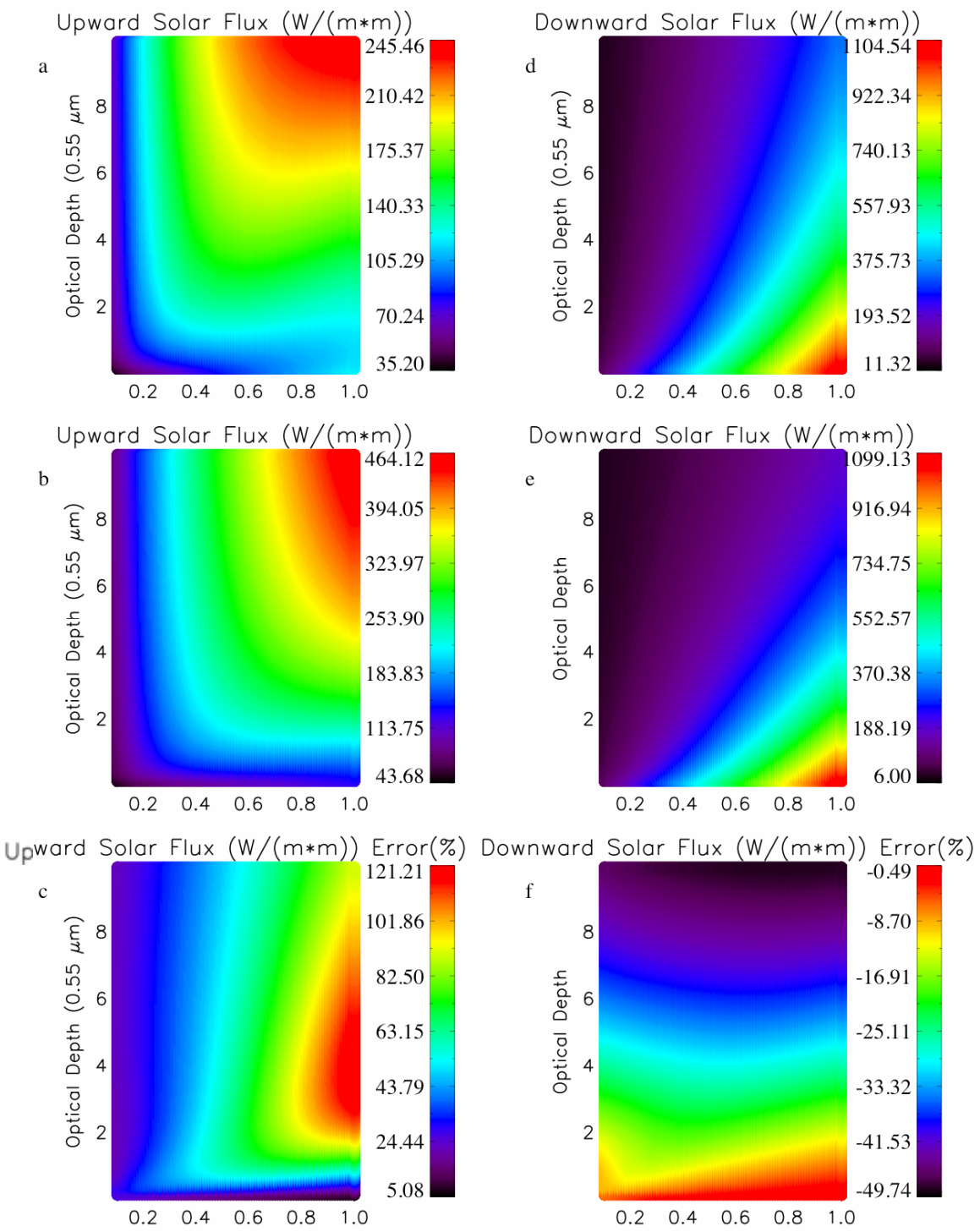

Figure 37 Same as Figure 35 except that the size distribution is in the mid-latitude regions and the range of the optical depth (0.55 m) is from 0.1 to 10

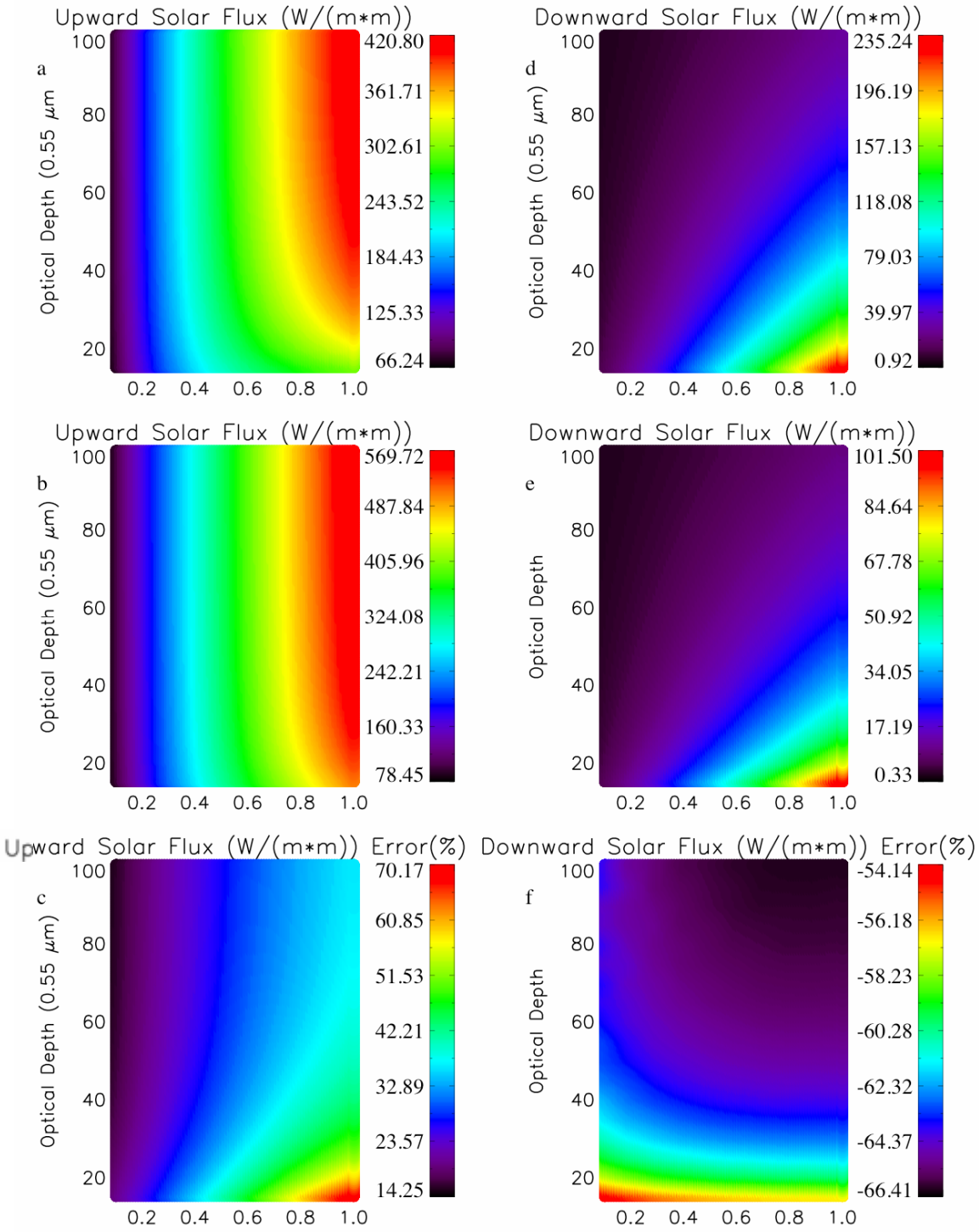

Figure 38 Same as Figure 35 except that the size distribution is in the mid-latitude regions and the range of the optical depth (0.55 m) is from 10 to 100

decrease as cosine of solar zenith angle increases; when $\tau_{0.55}$ is larger than 4, the underestimation exaggerates as cosine of solar zenith angle increases.

Figures 37 and 38 are the same as Figs. 35 and 36 except for the mid-latitude cirrus clouds. The relative differences in Figs. 37c, 38c and Figs. 37f, 38f are similar to those in Figs. 35c, 36c and Figs 35f, 36f, while the relative differences in Figs. 37 and 38 are larger.

4.4 Net heating rates

Figures 39 and 40 show the net heating rates and their relative errors with the simulated and reference optical properties, when $\tau_{0.55}$ ranges from 0.1 to 100 and solar zenith angle is equal to 1. In the Figs. 39 and 40, it is evident that the heating effects of cirrus clouds and the ozone layer high in the atmosphere. The relative errors of the heating rates for mid-latitude cirrus clouds are shown in Figs. 39c and 40c. The entire heating rates profiles with simulated bulk optical properties match very well with those with the reference optical properties. For the layers without clouds, including TOA and surface, the maximum error is 0.47%. The existence of cirrus clouds heats the surrounding atmosphere significantly and the relative errors due to the underestimation of simulated absorption efficiency emerge. When $\tau_{0.55}$ grows from 0.1 to 100, the relative errors of heating rates decrease from 1.16% to -25.96%. Figs. 39f and 40f illustrates the relative errors of heating rates in tropical cirrus cloud case. In Figs. 39 and 40, the relative errors in (f) and (c) are similar. The relative errors of heating rates for tropical case range from 1.04% to -26.20% in the layer with clouds.

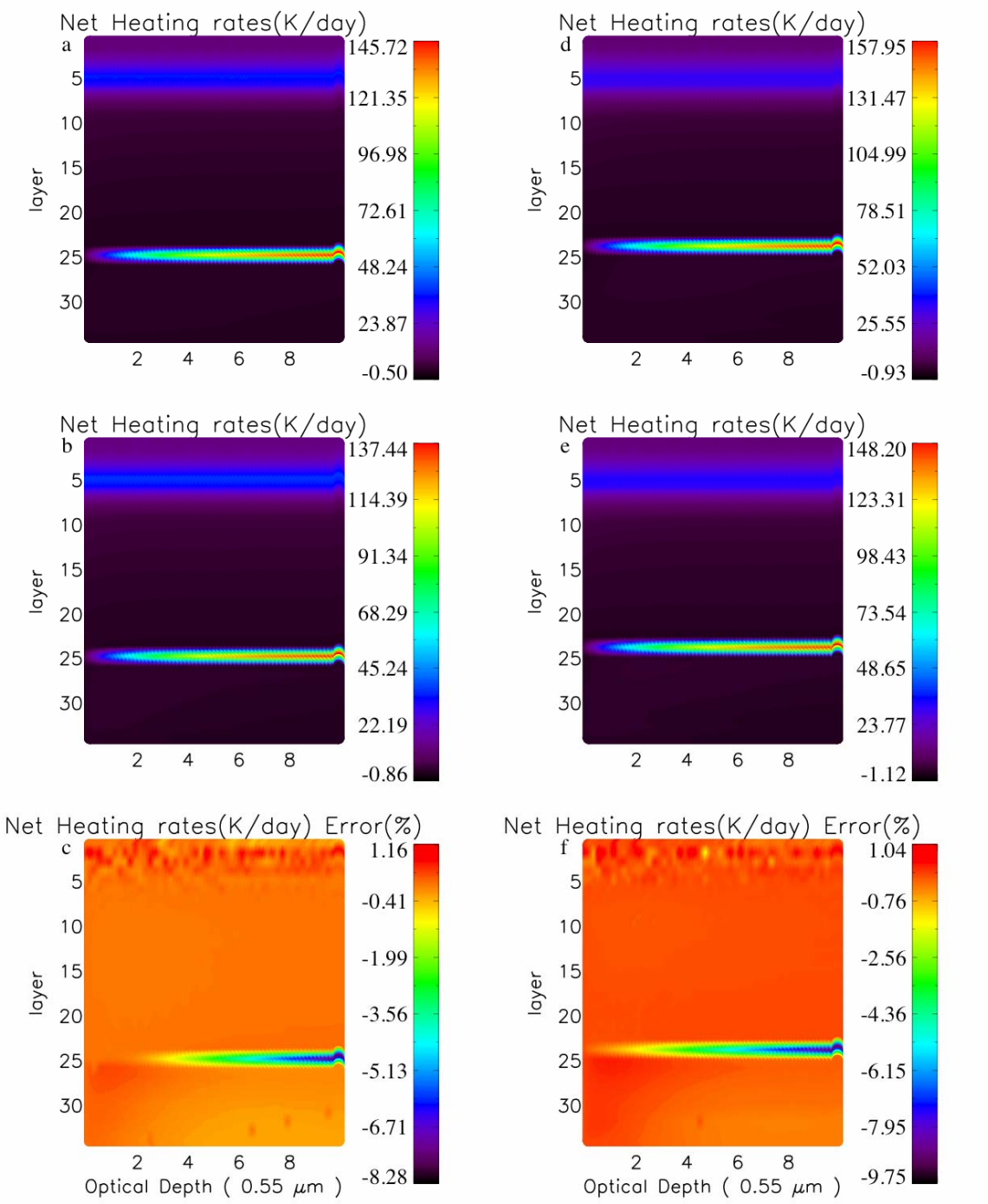

Figure 39 Heating rates and their relative errors when the range of the optical depth (0.55 m) is from 0.1 to 10 and solar zenith angle is 1.0; (a) and (d) are from the IGOM-based data; (b) and (e) heating rates are from the ADT-based method; (c) and (f) relative errors between the ADT-based and the IGOM-based data. The left three panels are with the size distribution at mid-latitudes and the three panels on the right side are with the size distribution at tropics

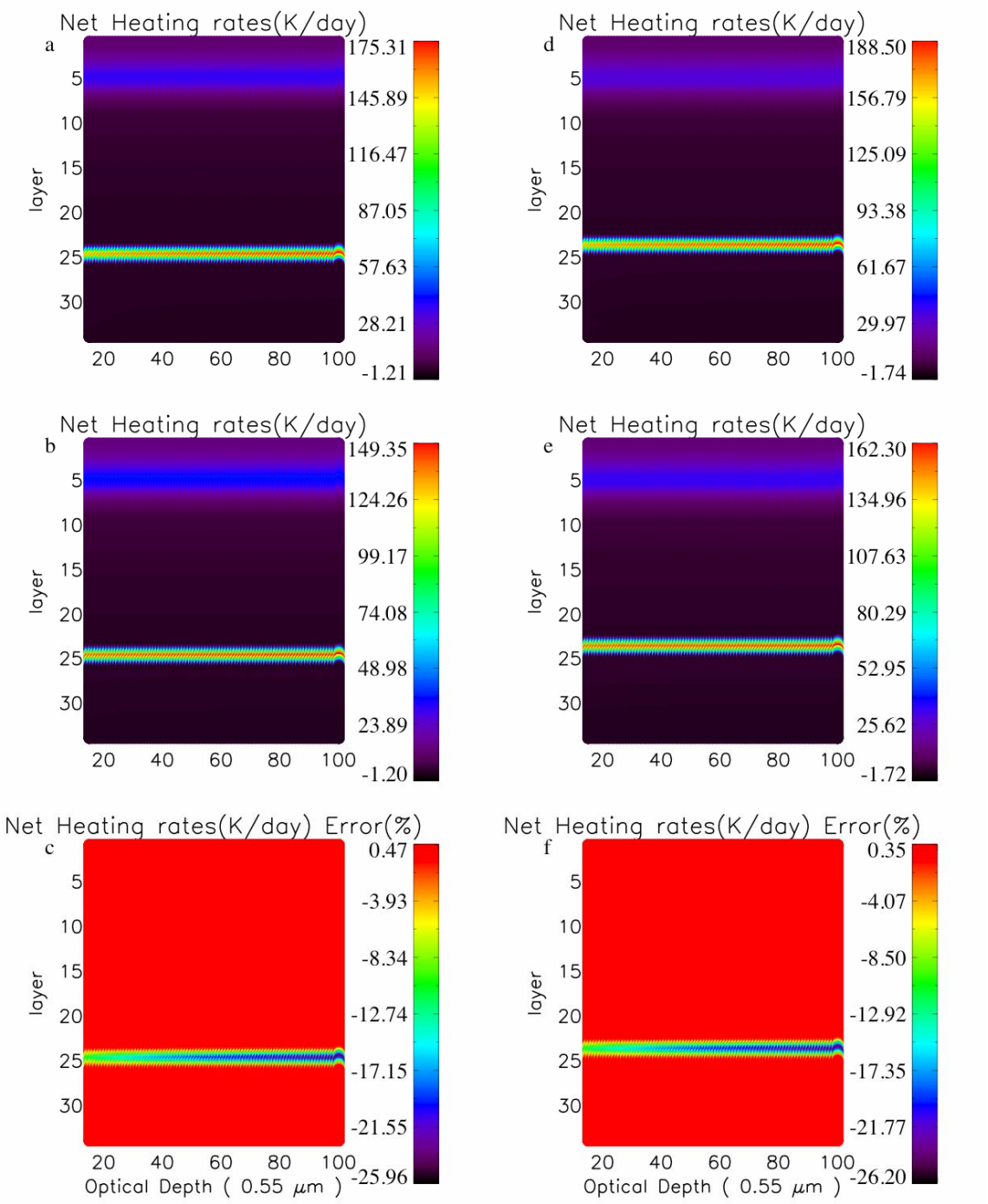

Figure 40 Same as Figure 39 except that the range of the optical depth (0.55 m) is from 10 to 100

5. CONCLUSIONS

The original anomalous diffraction theory requires two assumptions: the refractive index of the particle m is close to 1; the size parameter x is much larger than 1. By considering the first order reflection, the absorption efficiency of particles will be more accurate in the large size parameter cases even when m is not near 1. The asymmetry factors, which fit well in the IR regions, are derived. Improvements are still needed in the solar region.

The preset simulations compute the single-scattering properties of six non-spherical ice particles, which are droxtals, 6-branch bullet rosettes, solid hexagon columns, hollow hexagons columns, aggregates and plates. To better understand the accuracy, the database of a rigorous method IGOM is applied (Yang et al., 2000; 2005). For the single scattering properties of 6 non-spherical ice crystals, we have the following conclusions:

1) The extinction efficiency is quite accurate in both solar regions and IR regions. The shorter the wavelength is, the better the simulated results match with the reference results. When in the longwave region and when the size parameter is small, the ADT-based method will generate small errors. That is because that in the modified ADT assumptions, the ray passes the scattering particles without the propagation direction changes. It is also noticeable that the shape factors of non-spherical particles are quite important to the underestimation errors of extinction efficiency.

2) The simulations based on ADT can generate good absorption efficiency of the six non-spherical ice particles. The consideration of the first-order reflection makes the absorption efficiency works perfect when the size parameter is large. The absorption

efficiency in the shortwave region is close to 0, and in the near infrared and the IR regions, the errors between ADT-based and IGOM-based results are under 15% when the size parameter is larger than 30.

3) The phase functions are derived. The ADT-based method can generate quite accurate asymmetry factors in the IR region and the near-IR region when the absorption is strong. However, in the solar parts (0.5 μm and 1.23 μm), some improvements are still needed.

We then examine the errors in radiative properties by applying the simulated and reference optical properties of non-spherical ice particles in the Fu-Liou model. Two cases are designed: one case is to simulate tropical cirrus clouds and the other one is to simulate mid-latitude cirrus clouds.

It is evident that upward IR fluxes and downward solar fluxes are underestimated; however, the downward IR fluxes and upward solar fluxes are overestimated. These errors result from the underestimation of the estimated bulk asymmetry factor. The ultimate relative errors of downward IR fluxes and upward IR fluxes in both cases are 29.5% and -18.31%, respectively. It is noted that relative errors the upward IR fluxes at TOA we found that the values are basically under 5.0 %; and the relative differences of downward IR fluxes at surface are all under 5.0 %. Thus, ADT-based single scattering properties of six non-spherical shapes could be used to calculate the IR radiative fluxes at TOA and surface with a reasonably error. In the solar region, the relative errors of the upward solar fluxes basically increase with the optical depth at 0.55um. For the upward solar flues at TOA, the relative errors between ADT-base and IGOM-based are about 20%. The relative errors of downward solar fluxes at surface increase from 6.36% to 65% for the mid-latitude case and about 4% to 50% as the optical depth increases. As a result,

the ADT-based single scattering properties can only apply to the computation of solar fluxes when the optical depth is large or the cosine of solar zenith angle is small. Net heating rates are also examined and the heating effects of cirrus clouds on the surrounding atmosphere are found significant. The net heating rates based on ADT are found to be smaller than those based on IGOM and the errors are mainly caused by underestimation of ADT-based absorption efficiency. The relative errors of net heating rates decrease and can reach only -26.5% when $\tau_{0.55}$ is 100. Thus the ADT-based optical properties can be used to calculate heating rates with a good accuracy. In addition, comparing the radiative properties for the tropical cirrus clouds with those for the mid-latitude ones, we found that the relative errors for tropical cirrus clouds are smaller. Therefore the ADT-based single-scattering properties are more suitable for the application to the cirrus clouds in the tropical region.

In order to check the applications of ADT, the single-scattering properties based on ADT of six non-spherical ice crystals are applied to compute the radiative fluxes and heating rates of cirrus clouds. It is found that the errors of IR fluxes and net heating rates with ADT-based and IGOM-base optical properties are in a reasonable range and the differences of solar fluxes are significant and even can exceed 100%. Notably, the relatively large errors of asymmetry factors can influence the upward and downward fluxes in a limited range. Predictably, since radiative forcing is defined as the change of net fluxes (the difference between the incoming fluxes and outgoing fluxes), the effects of the accuracy of asymmetry factor should be emphasized. Also, in the study, the underestimation of absorption efficiency generates large errors to the fluxes when the cirrus clouds are optically transparent and limited errors on the net heating rates. In conclusion, ADT is a good approximation to compute the extinction and absorption

efficiencies. The underestimation of extinction and absorption efficiencies based on ADT can generate significant errors in the calculation of the radiative properties of cirrus clouds.

In the future, the edge effects and internal reflections should be considered to improve the accuracy of absorption efficiency. Moreover, refraction effects should be considered into the computation of the asymmetry factor.

REFERENCES

Baum, B. A., A. Heymsfield, P. Yang, and S. M. Thomas, 2005: Bulk scattering properties for the remote sensing of ice clouds, I: Microphysical data and models. *J. Appl. Meteor*., **44**, 1885-1895.

Chýlek, P., and D. K. James, 1991a: Extinction cross sections of non-spherical particles in the anomalous diffraction approximation. *J. Opt. Soc. Amer. A.,* **8**, 274-281, doi:10.1364/JOSAA.8.000274.

Chýlek, P., and D. K. James, 1991b: Absorption and scattering of electromagnetic radiation by prismatic columns: Anomalous diffraction approximation. *J. Opt. Soc. Am. A.*, **8**, 1713-1720.

Fu, Q., 1991: Parameterization of radiative processes in vertically non-homogeneous multiple scattering atmospheres. Ph.D. dissertation, University of Utah, Salt Lake City, 259 pp.

Fu, Q., 1996: An accurate parameterization of the solar radiative properties of cirrus clouds for climate models. *J. Climate*, **9**, 2058-2082.

Fu, Q., and W. Sun, 2001: Mie Theory for light scattering by a spherical particle in an absorbing medium. *Appl. Opt*., **40**, 1354-1361.

Heymsfield, A. J., 1975a: Cirrus uncinus generating cells and the evolution of cirriform clouds. Part I: Aircraft observations of the growth of the ice phase. *J. Atmos. Sci*., **32**, 798-808.

Heymsfield, A. J., 1975b: Cirrus uncinus generating cells and the evolution of cirriform clouds. Part II: The structure and circulations of the cirrus uncinus generating head. *J. Atmos. Sci.*, **32**, 809-819.

Heymsfield, A. J., 1975c: Cirrus uncinus generating cells and the evolution of cirriform clouds. Part III: Numerical computations of the growth of the ice phase. *J. Atmos. Sci*., **32**, 820-830.

Heymsfield, A. J., and R. G. Knollenberg, 1972: Properties of cirrus generating cells. *J. Atmos. Sci.*, **29**, 1358-1366.

Hobbs, P. V., L. F. Radke, and D. G. Atkinson, 1975: Airborne measurements and observations in cirrus clouds. AFCRL-TR-75-0249, Air Force Geophysics Laboratory, Hanscom AFB, 117pp.

Liou, K. N., 1986: Influence of cirrus clouds on weather and climate processes: A global perspective. *Mon. Wea. Rev.*, **114**, 1167-1199.

Liu, Y., W. P. Arnott, and J. Hallet, 1998: Anomalous diffraction theory for arbitrarily orientated finite circular cylinders and comparison with exact T-matrix result. *Appl. Opt.*, **37**, 5019–5030.

Mishchenko, M. I., L. D. Travis, and D. W. Mackowski, 1996a: T-matrix computations of light scattering by nonspherical particles: A review. *J. Quan. Spectro. Rad. Transfer,* **55**, 535-575.

Mishchenko, M. I., W. B. Rossow, A. Macke, and A. A. Lacis, 1996b: Sensitivity of cirrus cloud albedo, bidirectional reflectance and optical thickness retrieval accuracy to ice particle shape. *J. Geophys. Res.*, **101**, 16973–16985.

Mitchell, D. L., 2000: Parameterization of the Mie extinction and absorption coefficients for water clouds. *J. Atmos. Sci.*, **57**, 1311– 1326.

Sassen, K., and K. N. Liou, 1979: Scattering of polarized laser light by water droplet, mixed-phase and ice-crystal clouds. Part I: Angular scattering patterns. *J. Atmos. Sci*., **36**, 838-851.

Stephen, G. W., and R. E. Brandt, 2008: Optical constants of ice from the ultraviolet to the microwave: A revised compilation. *J. Geophys. Res*., **113**, D14220, doi: 10.1029/2007JD009744.

Sunilkumar, S. V., K. Parameswaran, and B. V. Thampi, 2008: Interdependence of tropical cirrus properties and their variability. *Ann. Geophys*., **26**, 413-429.

van de Hulst, H. C., 1957: *Light Scattering by Small Particles*. Wiley.

Varley, D. J., I. D. Cohen, and A. A. Barnes, 1980: Cirrus particle distribution study. Part VII. AFGL-TR-80-0324, Air Force Geophysics Laboratory, Hanscom AFB, 82 pp.

Warren, S. G., and R. E. Brandt, 1984: Optical constants of ice from the ultraviolet to the microwave, *Appl. Opt*., **23**, 1206-1225.

Weickmann, H. K., 1945: Formen und buldung atmopharisher eiskristalle. Beitr. *Phys. Atmos.*, **28**, 12-52.

Yang, P., B. A. Baum, A. J. Heymsfield, Y. X. Hu, H.L. Huang, S.-Chee Tsay, and S. Ackerman, 2003: Single-scattering properties of droxtals. *J. Quant. Spectrosc. Radiat. Transfer,* **79-80**, 1159-1180.

Yang, P., and K. N. Liou, 1995: Light scattering by hexagonal ice crystals: Comparison of finite-difference time domain and geometric optics methods. *J. Opt. Soc. Amer. A.,* **12**, 162-176.

Yang, P., and K. N. Liou, 1997: Light scattering by hexagonal ice crystals: Solution by ray-by-ray integration algorithm. *J. Opt. Soc. Amer. A.*, **14**, 2278-2289.

Yang, P., K. N. Liou, K. Wyser, and D. Mitchell, 2000: Parameterization of the scattering and absorption properties of individual ice crystals. *J. Geophys. Res*., **105**, 4699-4718.

Yang, P., Z. Zhang, B. A. Baum, H. L. Huang, and Y. Hu, 2004: A new look at anomalous diffraction theory (ADT): Algorithm in cumulative projected-area

distribution domain and modified ADT. *J. Quant. Spectrosc. Radiat. Transfer*, **89**, 421-442.

Yang, P., H. Wei, H.-L. Huang, B. A. Baum, Y. X. Hu, G. W. Kattawar, M. I. Mishchenko, and Q. Fu, 2005: Scattering and absorption property database for nonspherical ice particles in the near- through far-infrared spectral region. *Appl. Opt.*, **44**, 5512-5523.

Yue, Q., and K. N. Liou, (2009): Cirrus cloud optical and microphysical properties determined from AIRS infrared spectra. *Geophys. Res. Lett.*, **36**, L05810, doi:10.1029/2008GL036502.

Zhang, Y., A. Macke, and F. Albers, 1999: Effect of crystal size spectrum and crystal shape on stratiform cirrus radiative forcing. *Atmos. Res.,* **52**, 59-75.

VITA

Kai Lu received his Bachelor of Science degree in physics at Nanjing University of Information Science and Technology in Nanjing in June 2008. He continued his study in the Department of Atmospheric Sciences at Texas A&M University beginning in September 2008 and received his Master of Science degree in August 2010.

After graduation, Mr. Lu will return to China. His department email address is hyoga@ariel.met.tamu.edu. Permanent mailing address is Department of Atmospheric Sciences, MS 3150, Texas A&M University, College Station, Texas 77843-3150.